https://doi.org/10.61092/iaea.wx80-dm11

INDC(NDS)-0864
Distr. J,RD,ST

IAEA
International Atomic Energy Agency

INDC International Nuclear Data Committee

Observations on the Effects of ^{252}Cf Spontaneous-Fission Neutron Spectrum Uncertainties on Uncertainties in Calculated Spectrum-Average Cross Sections for Reactions in the Neutron Dosimetry Library IRDFF-II

Donald L. Smith
Argonne National Laboratory (retired)
231 Hawthorne Walk
Chula Vista, CA 92118, U.S.A.

November 2022

IAEA Nuclear Data Section
Vienna International Centre, P.O. Box 100, 1400 Vienna, Austria

Selected INDC documents may be downloaded in electronic form
from *http://nds.iaea.org/publications*
or sent as an e-mail attachment.
Requests for hardcopy or e-mail transmittal should be directed to
NDS.Contact-Point@iaea.org
or to
Nuclear Data Section
International Atomic Energy Agency
Vienna International Centre
P.O. Box 100
1400 Vienna
Austria

Printed by the IAEA in Austria

November 2022

INDC(NDS)-0864
Distr. J,RD,ST

Observations on the Effects of ^{252}Cf Spontaneous-Fission Neutron Spectrum Uncertainties on Uncertainties in Calculated Spectrum-Average Cross Sections for Reactions in the Neutron Dosimetry Library IRDFF-II

Donald L. Smith
Argonne National Laboratory (retired)
231 Hawthorne Walk
Chula Vista, CA 92118, U.S.A.

ABSTRACT

The Neutron Dosimetry Library IRDFF-II was released in January 2020, and was subsequently documented by an article published in the Nuclear Data Sheets by A. Trkov et al. The development of this library, under the auspices of the IAEA Nuclear Data Section, entailed extensive effort to assemble and examine the available, relevant experimental data, as well as to select and validate the best available cross-section evaluations, for some 110 neutron reaction processes included in this library. Part of the validation process for this library entailed comparing experimental and evaluated differential cross-sections as well as corresponding integral cross sections for a variety of integral neutron spectra considered to be relevant for fission and fusion neutron dosimetry purposes. Prominent among these spectra is the well-known ^{252}Cf spontaneous-fission (s.f.) neutron spectrum that is considered to be a standard for both IRDFF-II and the ENDF/B libraries. Experimental and calculated uncertainties for all these data were considered in this validation process. The evaluated ^{252}Cf s.f. neutron spectrum, owing to the manner in which it was developed, is considered to be largely independent of the evaluated neutron reaction cross sections in both of these libraries. Therefore, the uncertainties in calculated spectrum-average cross sections (SACS) stemming from evaluated cross-section uncertainties are considered to be largely independent from the uncertainties in the evaluated ^{252}Cf s.f. neutron-spectrum itself. The present investigation sought specifically to examine systematic behaviors for the uncertainties of calculated neutron reaction SACS in IRDFF-II due exclusively to uncertainties in the ^{252}Cf spectrum. This work was enabled by the availability of extensive calculations performed and documented by A. Trkov during development of the IRDFF-II Library. It was observed from the present investigation that the ^{252}Cf s.f. neutron spectrum component of these calculated SAC uncertainties, for threshold reactions that exhibit relatively smooth cross-section behaviors, vary quite smoothly and predictably as a function of the parameter $E_{50\%}$ (that neutron energy at which the reaction-rate integral for this neutron spectrum reaches 50% of the integral over the full energy range) for values of $E_{50\%}$ from around 2 MeV up to almost 17 MeV. The behaviors observed in the present investigation for those reactions in IRDFF-II involving lower and higher values of $E_{50\%}$ are less predictable owing to factors that are discussed in this report. This report also provides numerous tables and plots based on calculated results from the work of A. Trkov to illustrate these conclusions.

November 2022

Contents

1. Introduction

IRDFF-II is the most-recent updated version (released in January 2020) of a neutron dosimetry library that is widely employed by the fission and fusion reactor dosimetry community [1]. This new library has been documented in detail in an article that was concurrently published in the Nuclear Data Sheets [2]. The content of the IRDFF-II library is indicated in the following abstract which has been extracted in verbatim from this article:

"*The new IRDFF-II library includes 119 metrology reactions, four cover material reactions to support self-shielding corrections, five metrology metrics used by the dosimetry community, and cumulative fission products yields for seven fission products in three different neutron energy regions. In support of characterizing the measurement of the residual nuclei from the dosimetry reactions and the fission product decay modes, the present document lists the recommended decay data, particle emission energies and probabilities for 68 activation products. It also includes neutron spectral characterization data for 29 neutron benchmark fields for the validation of the library contents. Additional six reference fields were assessed (four from plutonium critical assemblies, two measured fields for thermal-neutron induced fission on* ^{233}U *and* ^{239}Pu *targets) but not used for validation due to systematic discrepancies in C/E reaction rate values for lack of reaction-rate experimental data. Another ten analytical functions are included that can be useful for calculating average cross sections, average energy, thermal spectrum average cross sections and resonance integrals.*"

Comparisons of experimental differential cross-section data to comparable evaluated results from IRDFF-II are discussed in this library's documentation [1,2]. Also, comparisons are made to relevant experimental and calculated spectrum-average cross-sections (SACS) for a variety of benchmark neutron fields, including the ^{252}Cf s.f. neutron field $\phi(E)$ whose spectrum is so well known that it is treated as a standard in both IRDFF-II and ENDF/B-VIII.0 [1–4]. Evaluated differential cross sections $\sigma(E)$ from IRDFF-II were used in all of these calculations. Uncertainties stemming from both reaction-cross-section uncertainties and spectrum-characterization uncertainties were determined for most of these data. Comparisons of uncertainties for the different reactions are based on calculations that utilize the computed quantity $E_{50\%}$ to standardize these comparisons. $E_{50\%}$ is defined symbolically by the formula

$$\int\{0,E_{50\%}\}\ \sigma(E)\ \phi(E)\ dE = \int\{E_{50\%},\infty\}\ \sigma(E)\ \phi(E)\ dE = 0.5\ . \qquad (1)$$

The notation " $\int\{\ldots\}$ " signifies integration between the limits 0 and $E_{50\%}$ or $E_{50\%}$ and ∞, respectively. Therefore, $E_{50\%}$ is interpreted as that neutron energy at which the reaction-rate integral for the neutron spectrum reaches 50% of the integral over the full energy range. This is a reasonable parameter to use in comparing SACS data for diverse reactions since in each reaction half of the contributed yield to the SACS occurs from energies below $E_{50\%}$ whereas half of the contribution comes from energies above $E_{50\%}$, as is clearly evident in Eq. (1).

In particular, information pertinent to ^{252}Cf s.f. spectrum SACS is given for 44 selected cases in Table XVIII of [2]. Since the evaluated data for this spectrum and for the reaction cross sections in IRDFF-II are considered to be largely independent [2,5], estimated SACS uncertainties attributable to cross-section and spectrum uncertainties can be examined separately (see the formalism in Appendix). This is exemplified in this table by the appearance of total SACS uncertainties and SACS uncertainties attributed to cross-section uncertainties shown in separate columns. From this table, estimates conceivably could be made of the spectrum-related uncertainty contributions to the total SACS uncertainties. However, such estimates that might be deduced from this table would not be sufficiently precise for those data exhibiting relatively small values of $E_{50\%}$ since the uncertainty components stemming from the

spectrum alone are clearly also small in this region, and the number of significant figures used for the numerical data presented in the table are inadequate for this purpose. Values for ^{252}Cf s.f. neutron spectrum SACS uncertainties given in Table XVIII were calculated using code RR_UNC that was developed by A. Trkov [2,6,7]. Furthermore, a more extensive printout from a particular run with this code for the IRDFF-II cross-section data set is available for open inspection [7,8]. Uncertainty components in SACS data attributable to the computed ^{252}Cf s.f. neutron spectrum uncertainties that are provided explicitly in the printout for 110 cases appear with adequate numerical precision for meaningful analysis. The complete printout is reproduced in Table I below.

It is important to recognize that the numerical representation of the ^{252}Cf s.f. neutron spectrum used in the calculations performed by code RR_UNC must be normalized. That is, the integral of spectrum $\phi(E)$ over all neutron energies E (or in the case of a discrete group representation the sum of spectrum group fluxes) must be unity (see discussion in Appendix). This must also be reflected in the spectrum covariance matrix that represents the spectrum uncertainties and correlations.

2. Examination of the Data and Observations

As mentioned earlier, Table I reproduces the above-mentioned printout from computer code RR_UNC. Heading labels are described at the end of this table. Be advised that in this printout (and elsewhere in this report) E (50%) has the same meaning as $E_{50\%}$, so they are used interchangeably. Examination of the entries in Table I reveals that for data point Nos. 52, 64, and 82, the values of $E_{50\%}$ given in Table I are all equal to zero. This is unrealistic, so these entries from Table I are considered no further in the present investigation. In Table II, information from Table I that is pertinent to the present investigation (excluding data point Nos. 52, 64, and 82) is presented in an Excel spreadsheet, including identification of the reactions for each entry. These entries are organized in ascending order from lowest values of energy $E_{50\%}$ to the highest values of $E_{50\%}$. The original line number identifiers shown in Table I (and indicated by the heading "No.") are retained, but in Table II they now appear in non-sequential order. The reader will also notice that several lines in Table II are highlighted. On careful inspection, it can be observed that in such instances the highlighted lines appear in adjacent pairs. For each of these pairs, the values of E (50%) MeV and Unc. Sp. [%] are seen to be essentially identical. These paired, adjacent rows in Table II correspond to basically the same reaction process. Therefore, they are redundant for present purposes. The essential information for the present investigation can be retained by eliminating duplications and reducing each pair to a single line. Table III presents the same information found in Table II with such redundancies eliminated. The single retained data point from each of the redundant pairs remains highlighted in Table III.

Table I: Printout consisting of two pages produced by computer code RR_UNC (A. Trkov) [6,8]). Column headings appearing in the table are identified at the bottom of the table. Some of these codes correspond to those defined in the ENDF-6 Formats Manual [9].

```
RR_UNC - Calculate uncertainties in reaction rates
-----------------------------------------------------------
Andrej Trkov, Jozef Stefan Institute, Ljubljana, Slovenia
                 Version Jul. 2019
-----------------------------------------------------------

Reference x.s. file      : group_files\IRDFF-II.g
Source spectrum file     : spectra\Cf252sf.g
Reaction rate integ.flag :      1
Reaction rate norm. flag :      1

Spectrum MAT No.         :   9861
Spectrum Integral            :  1.000E+00
Spectrum average energy [eV] :  2.121E+06
Spectrum peak energy    [eV] :  7.397E+05
Reaction rate RR = average cross-section
```

No.	Mat.	MT	E(50%) [MeV]	<RR> +/- Unc [mb]	Unc. x.s. [%]	Unc. Sp. [%]	Unc. Total [%]
3	3000	205	4.00588	4.8236E+01 +/- 6.691E-01	1.22	.66	1.39
4	3000	207	4.08303	6.0521E+01 +/- 2.545E+00	4.16	.65	4.21
7	3006	105	.65237	3.2063E+02 +/- 2.698E+00	.64	.55	.84
8	3006	205	.65237	3.2063E+02 +/- 2.698E+00	.64	.55	.84
9	3006	207	1.70993	4.8215E+02 +/- 3.242E+01	6.71	.40	6.72
12	3007	205	6.00574	2.5863E+01 +/- 6.913E-01	2.37	1.23	2.67
13	3007	207	6.00577	2.5891E+01 +/- 6.914E-01	2.37	1.23	2.67
17	5000	205	3.73676	1.0250E+01 +/- 1.227E+00	11.96	.51	11.97
18	5000	207	1.4856	1.0936E+02 +/- 9.275E+00	8.47	.44	8.48
22	5010	107	.89788	4.3938E+02 +/- 4.736E+01	10.76	.57	10.78
23	5010	205	3.73456	5.1465E+01 +/- 6.168E+00	11.97	.51	11.99
24	5010	207	1.47677	5.4790E+02 +/- 4.662E+01	8.50	.44	8.51
25	5010	800	1.81743	1.8424E+02 +/- 4.532E+01	24.60	.20	24.60
26	5010	801	.42562	2.5514E+02 +/- 2.127E+01	8.27	1.01	8.33
29	5011	205	12.8385	1.0895E-02 +/- 1.886E-03	17.01	3.22	17.31
30	5011	207	11.4595	4.1587E-01 +/- 6.256E-02	14.87	2.27	15.04
31	9019	16	14.0522	1.6335E-02 +/- 8.979E-04	2.90	4.67	5.50
34	11023	16	15.5953	8.5729E-03 +/- 7.305E-04	1.28	8.43	8.52
35	11023	102	1.00585	2.7523E-01 +/- 1.069E-02	3.80	.83	3.88
36	12000	11024g	8.26095	1.6608E+00 +/- 2.958E-02	.80	1.59	1.78
37	12024	103	8.26047	2.1020E+00 +/- 3.744E-02	.80	1.59	1.78
38	13027	16	16.1556	7.7247E-03 +/- 8.647E-04	3.54	10.62	11.19
39	13027	103	5.84274	4.7445E+00 +/- 1.116E-01	2.05	1.15	2.35
40	13027	107	8.66807	1.0167E+00 +/- 1.804E-02	.71	1.63	1.77
41	13027	11024g	8.66807	1.0167E+00 +/- 1.804E-02	.71	1.63	1.77
42	13027	13026g	15.9694	6.8607E-03 +/- 6.958E-04	3.81	9.40	10.14
43	14000	13028g	7.22591	6.5546E+00 +/- 1.871E-01	2.47	1.43	2.85
44	14028	103	7.2258	7.1069E+00 +/- 2.029E-01	2.47	1.43	2.85
45	14029	13028g	16.106	9.2743E-03 +/- 1.087E-03	4.45	10.85	11.72
46	15031	103	3.73196	3.8009E+01 +/- 1.323E+00	3.42	.65	3.48
47	16000	15032g	4.07413	7.0307E+01 +/- 1.818E+00	2.48	.72	2.59
48	16032	103	4.07412	7.4015E+01 +/- 1.914E+00	2.48	.72	2.59
51	21045	102	.56682	4.9078E+00 +/- 4.471E-01	9.05	1.07	9.11
52	22000	21046g	0	1.1411E+00 +/- 3.733E-02	3.05	1.19	3.27
53	22046	16	16.1202	1.2585E-02 +/- 1.376E-03	4.23	10.08	10.94
54	22046	103	6.08127	1.3814E+01 +/- 4.524E-01	3.05	1.19	3.28
55	22047	103	3.81716	1.9533E+01 +/- 5.471E-01	2.73	.61	2.80
56	22048	103	8.35358	4.2637E-01 +/- 2.358E-02	5.30	1.57	5.53
57	23051	107	9.97529	3.8552E-02 +/- 1.374E-03	3.02	1.89	3.56
58	23051	21048g	9.97529	3.8552E-02 +/- 1.374E-03	3.02	1.89	3.56
59	24000	24051g	14.7195	8.1788E-02 +/- 5.298E-03	2.68	5.90	6.48
62	25055	16	12.9165	4.7290E-01 +/- 1.853E-02	2.32	3.16	3.92
63	25055	102	.74967	2.8100E+00 +/- 7.798E-01	27.72	1.33	27.75
64	26000	24051g	0	6.4974E-02 +/- 2.514E-03	3.60	1.42	3.87
67	26054	16	16.6092	3.6640E-03 +/- 4.719E-04	5.00	11.87	12.88
68	26054	103	4.43835	8.6449E+01 +/- 2.734E+00	3.06	.81	3.16
69	26054	107	7.42963	1.1116E+00 +/- 4.302E-02	3.60	1.42	3.87

70	26056	103	7.57906	1.4626E+00	+/-	4.364E-02	2.60	1.46	2.98
73	26058	102	.73382	2.0143E+00	+/-	2.220E-01	11.00	.65	11.02
76	27059	16	13.0897	4.0779E-01	+/-	1.493E-02	1.52	3.33	3.66
77	27059	17	22.3768	9.8020E-05	+/-	7.458E-05	7.31	75.74	76.09
78	27059	102	.90285	4.8642E+00	+/-	2.031E-01	4.08	.90	4.17
79	27059	103	5.94299	1.7132E+00	+/-	6.246E-02	3.46	1.16	3.65
80	27059	107	8.37156	2.2097E-01	+/-	8.555E-03	3.54	1.56	3.87
81	27059	25056g	8.37156	2.2097E-01	+/-	8.555E-03	3.54	1.56	3.87
82	28000	27058g	0	7.9864E+01	+/-	1.506E+00	1.74	.74	1.89
83	28058	16	14.9857	8.6453E-03	+/-	5.874E-04	1.29	6.67	6.79
84	28058	103	4.20306	1.1731E+02	+/-	2.213E+00	1.74	.74	1.89
85	28060	103	7.05428	2.7985E+00	+/-	6.344E-02	1.81	1.37	2.27
86	29000	27060g	7.27355	4.7887E-01	+/-	1.569E-02	2.97	1.38	3.28
89	29063	16	13.8404	1.9874E-01	+/-	8.954E-03	1.38	4.29	4.51
90	29063	102	.96389	1.0409E+01	+/-	8.780E-01	8.41	.62	8.44
91	29063	107	7.27355	6.9251E-01	+/-	2.270E-02	2.97	1.38	3.28
92	29065	16	12.6796	6.5334E-01	+/-	2.299E-02	1.89	2.97	3.52
93	30000	29064g	4.16697	2.0970E+01	+/-	3.900E-01	1.69	.78	1.86
94	30064	103	4.16697	4.2647E+01	+/-	7.932E-01	1.69	.78	1.86
95	30067	103	4.70905	1.1054E+00	+/-	5.873E-02	5.25	.81	5.31
98	30068	29067g	15.5657	2.6534E-03	+/-	4.698E-04	14.68	9.91	17.71
99	33075	16	12.9142	6.2024E-01	+/-	4.072E-02	5.75	3.17	6.56
100	39089	16	13.9015	3.4591E-01	+/-	1.567E-02	1.24	4.35	4.53
101	40000	40089g	14.424	1.1215E-01	+/-	6.049E-03	.91	5.32	5.39
102	40090	16	14.4235	2.1793E-01	+/-	1.174E-02	.91	5.31	5.39
105	41093	102	.65159	2.4214E+01	+/-	5.760E-01	2.19	.92	2.38
106	41093	41093m	2.68481	1.4603E+02	+/-	3.809E+00	2.59	.35	2.61
107	41093	41092m	11.3282	7.8986E-01	+/-	1.883E-02	.84	2.23	2.38
108	41093	41094g	.65159	6.0471E+00	+/-	1.438E-01	2.19	.92	2.38
109	42000	41092m	5.39115	1.1368E+00	+/-	4.258E-02	3.60	1.02	3.75
110	42092	41092m	5.39114	7.8236E+00	+/-	2.931E-01	3.60	1.02	3.75
111	45103	45103m	2.37843	7.2452E+02	+/-	2.859E+01	3.94	.25	3.95
114	47109	47110n	.73434	9.3470E+00	+/-	7.079E-01	7.55	.53	7.57
118	49000	49114m	1.36123	8.9112E+00	+/-	2.568E-01	2.84	.46	2.88
122	49113	49113m	2.73029	1.5799E+02	+/-	1.963E+00	1.18	.39	1.24
123	49113	49114g	1.09394	4.2154E+01	+/-	1.362E+00	3.20	.46	3.23
127	49115	49115m	2.67343	1.9048E+02	+/-	3.243E+00	1.66	.37	1.70
128	49115	49114m	11.8082	1.6303E+00	+/-	8.981E-02	4.95	2.42	5.51
129	49115	49116g	1.04333	2.9565E+01	+/-	7.685E-01	2.57	.42	2.60
130	53127	16	11.5795	2.1027E+00	+/-	8.048E-02	3.03	2.33	3.83
133	57139	102	1.29321	6.6351E+00	+/-	3.386E-01	5.08	.48	5.10
134	59141	16	11.8459	1.9870E+00	+/-	2.255E-01	11.08	2.45	11.35
138	69169	16	10.382	6.2551E+00	+/-	2.360E-01	3.21	1.99	3.77
139	69169	17	18.4969	1.4740E-02	+/-	4.470E-03	5.76	29.77	30.32
142	73181	102	.81826	8.3464E+01	+/-	4.562E+00	5.41	.77	5.47
145	74186	102	1.02268	3.2794E+01	+/-	8.322E-01	2.50	.45	2.54
148	79197	16	10.5422	5.5213E+00	+/-	1.521E-01	1.87	2.02	2.75
149	79197	102	.72409	7.4978E+01	+/-	6.751E-01	.52	.74	.90
150	80199	80199m	3.09845	2.9594E+02	+/-	1.083E+01	3.63	.43	3.66
151	82204	82204m	5.04147	2.0374E+01	+/-	9.511E-01	4.57	.98	4.67
152	83209	16	9.86634	1.0016E+01	+/-	4.414E-01	3.99	1.87	4.41
153	83209	17	18.2255	1.9091E-02	+/-	5.199E-03	4.88	26.79	27.23
154	83209	37	26.6004	2.3173E-05	+/-	1.958E-05	37.49	75.74	84.51
155	83209	152	29.75	1.7437E-11	+/-	1.407E-11	27.82	75.74	80.69
158	90232	18	3.00637	8.3350E+01	+/-	4.830E+00	5.78	.42	5.80
159	90232	102	.90132	9.0055E+01	+/-	2.559E+00	2.81	.45	2.84
161	92235	18	1.70344	1.2267E+03	+/-	1.480E+01	1.21	.06	1.21
164	92238	16	8.20773	2.1092E+01	+/-	1.127E+00	5.10	1.60	5.34
165	92238	18	2.76849	3.2154E+02	+/-	4.136E+00	1.22	.39	1.29
166	92238	102	.91877	6.7424E+01	+/-	1.384E+00	2.00	.48	2.05
169	93237	18	2.0527	1.3598E+03	+/-	2.317E+01	1.69	.21	1.70
172	94239	18	1.77434	1.7978E+03	+/-	2.241E+01	1.25	.04	1.25
175	95241	18	2.22681	1.3966E+03	+/-	3.977E+01	2.83	.29	2.85

No.: Printout line number and unique data point identifier.

Mat.: Comparable to the ENDF-6 format MAT number which is equal to 1000*Z+A.

MT: Identifies the reaction type. Standard ENDF-6 format terms are used in this work, when applicable, otherwise codes that are unique to IRDFF-II are used as column headings.

E (50%): That neutron energy at which the neutron reaction-rate integral reaches 50% of the integral over the full energy range. The notation E (50%) is used interchangeably with $E_{50\%}$ in this report.

<RR>: Spectrum-average cross section (SACS) reaction rate in millibarn.

UNC: Uncertainty in the calculated integral SACS reaction rate in millibarn.

Unc. x.s.: Uncertainty in the calculated SACS due exclusively to cross-section uncertainties (in %).

Unc. Sp.: Uncertainty in the calculated SACS due exclusively to neutron-spectrum uncertainties (in %).

Table II. Data extracted from the printout generated by computer code RR_UNC (A. Trkov) [8] and transferred to an Excel spreadsheet (see Table I). Note that data point Nos. 52, 64, and 82 have been eliminated from this table for the reason discussed in the text of this report. The entries in this table are also sorted according to increasing values of E (50%).

No.	Mat.	MT	Reaction	E (50%) MeV	Unc. Sp. [%]	No.	Mat.	MT	Reaction	E (50%) MeV	Unc. Sp. [%]
26	5010	801	^{10}B(n,α_1)^{7}Li	0.4256	1	79	27059	103	^{59}Co(n,p)^{59}Fe	5.943	1.16
51	21045	102	^{45}Sc(n,γ)^{46}Sc	0.5668	1.1	12	3007	205	^{7}Li(n,^{4}He)^{3}H	6.006	1.23
105	41093	102	^{93}Nb(n,γ)^{94}Nb	0.6516	0.9	13	3007	207	^{7}Li(n,t)^{4}He	6.006	1.23
108	41093	41094g	^{93}Nb(n,γ)^{94g}Nb	0.6516	0.9	54	22046	103	^{46}Ti(n,p)^{46}Sc	6.081	1.19
7	3006	105	^{6}Li(n,t)^{4}He	0.6524	0.6	85	28060	103	^{60}Ni(n,p)^{60}Co	7.054	1.37
8	3006	205	^{6}Li(n,^{4}He)^{3}H	0.6524	0.6	44	14028	103	^{28}Si(n,p)^{28}Al	7.226	1.43
149	79197	102	^{197}Au(n,γ)^{198}Au	0.7241	0.7	43	14000	13028g	^{nat}Si(n,X)^{28g}Al	7.226	1.43
73	26058	102	^{58}Fe(n,γ)^{59}Fe	0.7338	0.7	91	29063	107	63Cu(n,α)αCo	7.274	1.38
114	47109	47110m	^{109}Ag(n,γ)^{110m}Ag	0.7343	0.5	86	29000	27060g	^{nat}Cu(n,X)^{60g}Co	7.274	1.38
63	25055	102	^{55}Mn(n,γ)^{56}Mn	0.7497	1.3	69	26054	107	^{54}Fe(n,α)^{51}Cr	7.43	1.42
142	73181	102	^{181}Ta(n,γ)^{182}Ta	0.8183	0.8	70	26056	103	^{56}Fe(n,p)^{56}Mn	7.579	1.46
22	5010	107	^{10}B(n,α)^{7}Li	0.8979	0.6	164	92238	16	^{238}U(n,2n)^{237}U	8.208	1.6
159	90232	102	^{232}Th(n,γ)^{233}Th	0.9013	0.5	37	12024	103	^{24}Mg(n,p)^{24}Na	8.26	1.59
78	27059	102	^{59}Co(n,γ)^{60}Co	0.9029	0.9	36	12000	11024g	^{nat}Mg(n,X)^{24g}Na	8.261	1.59
166	92238	102	^{238}U(n,γ)^{239}U	0.9188	0.5	56	22048	103	^{48}Ti(n,p)^{48}Sc	8.354	1.57
90	29063	102	^{63}Cu(n,γ)^{64}Cu	0.9639	0.6	80	27059	107	^{59}Co(n,α)^{56}Mn	8.372	1.56
35	11023	102	^{23}Na(n,γ)^{24}Na	1.0059	0.8	81	27059	25056g	^{59}Co(n,X)^{56g}Mn	8.372	1.56
145	74186	102	^{186}W(n,γ)^{187}W	1.0227	0.5	40	13027	107	^{27}Al(n,α)^{24}Na	8.668	1.63
129	49115	49116g	^{115}In(n,γ)^{116g}In	1.0433	0.4	41	13027	11024g	^{27}Al(n,X)^{24g}Na	8.668	1.63
123	49113	49114g	^{113}In(n,γ)^{114g}In	1.0939	0.5	152	83209	16	^{209}Bi(n,2n)^{208}Bi	9.866	1.87
133	57139	102	^{139}La(n,γ)^{140}La	1.2932	0.5	57	23051	107	^{51}V(n,α)^{48}Sc	9.975	1.89
118	49000	49114m	^{nat}In(n,γ)^{114m}In	1.3612	0.5	58	23051	21048g	^{51}V(n,X)^{48}Sc	9.975	1.89
24	5010	207	^{10}B(n,X)^{4}He	1.4768	0.4	138	69169	16	^{169}Tm(n,2n)^{168}Tm	10.38	1.99
18	5000	207	^{nat}B(n,X)^{4}He	1.4856	0.4	148	79197	16	^{197}Au(n,2n)^{196}Au	10.54	2.02
161	92235	18	^{235}U(n,fission)	1.7034	0.1	107	41093	41092m	^{93}Nb(n,2n)^{92m}Nb	11.33	2.23
9	3006	207	^{6}Li(n,X)^{4}He	1.7099	0.4	30	5011	207	^{11}B(n,X)^{4}He	11.46	2.27
172	94239	18	^{239}Pu(n,fission)	1.7743	0	130	53127	16	^{127}I(n,2n)^{126}I	11.58	2.33
25	5010	800	^{10}B(n,α_0)^{7}Li	1.8174	0.2	128	49115	49114m	^{115}In(n,2n)^{114m}In	11.81	2.42
169	93237	18	^{237}Np(n,fission)	2.0527	0.2	134	59141	16	^{141}Pr(n,2n)^{140}Pr	11.85	2.45
175	95241	18	^{241}Am(n,fission)	2.2268	0.3	92	29065	16	^{65}Cu(n,2n)^{64}Cu	12.68	2.97
111	45103	45103m	^{103}Rh(n,n')^{103m}Rh	2.3784	0.3	29	5011	205	^{11}B(n,X)^{3}H	12.84	3.22
127	49115	49115m	^{115}In(n,n')^{115m}In	2.6734	0.4	99	33075	16	^{75}As(n,2n)^{74}As	12.91	3.17
106	41093	41093m	^{93}Nb(n,n')^{93m}Nb	2.6848	0.4	62	25055	16	^{55}Mn(n,2n)^{54}Mn	12.92	3.16
122	49113	49113m	^{113}In(n,n')^{113m}In	2.7303	0.4	76	27059	16	^{59}Co(n,2n)^{58}Co	13.09	3.33
165	92238	18	^{238}U(n,fission)	2.7685	0.4	89	29063	16	^{63}Cu(n,2n)^{62}Cu	13.84	4.29
158	90232	18	^{232}Th(n,fission)	3.0064	0.4	100	39089	16	^{89}Y(n,2n)^{88}Y	13.9	4.35
150	80199	80199m	^{199}Hg(n,n')^{199m}Hg	3.0985	0.4	31	9019	16	^{19}F(n,2n)^{18}F	14.05	4.67
46	15031	103	^{31}P(n,p)^{31}Si	3.732	0.7	102	40090	16	^{90}Zr(n,2n)^{89}Zr	14.42	5.31
23	5010	205	^{10}B(n,X)^{3}H	3.7346	0.5	101	40000	40089g	^{nat}Zr(n,X)^{89g}Zr	14.42	5.32
17	5000	205	^{nat}B(n,X)^{3}H	3.7368	0.5	59	24000	24051g	^{nat}Cr(n,X)^{51g}Cr	14.72	5.9
55	22047	103	^{47}Ti(n,p)^{47}Sc	3.8172	0.6	83	28058	16	^{58}Ni(n,2n)^{57}Ni	14.99	6.67
3	3000	205	^{nat}Li(n,X)^{3}H	4.0059	0.7	98	30068	29067g	^{68}Zn(n,X)^{67g}Cu	15.57	9.91
48	16032	103	^{32}S(n,p)^{32}P	4.0741	0.7	34	11023	16	^{23}Na(n,2n)^{22}Na	15.6	8.43
47	16000	15032g	^{nat}S(n,X)^{32g}P	4.0741	0.7	42	13027	13026g	^{27}Al(n,2n)^{26g}Al	15.97	9.4
4	3000	207	^{nat}Li(n,X)^{4}He	4.083	0.7	45	14029	13028g	^{29}Si(n,X)^{28g}Al	16.11	10.9
94	30064	103	^{64}Zn(n,p)^{64}Cu	4.167	0.8	53	22046	16	^{46}Ti(n,2n)^{45}Ti	16.12	10.1
93	30000	29064g	^{nat}Zn(n,X)^{64g}Cu	4.167	0.8	38	13027	16	^{27}Al(n,2n)^{26}Al	16.16	10.6
84	28058	103	^{58}Ni(n,p)^{58}Co	4.2031	0.7	67	26054	16	^{54}Fe(n,2n)^{53}Fe	16.61	11.9
68	26054	103	^{54}Fe(n,p)^{54}Mn	4.4384	0.8	153	83209	17	^{209}Bi(n,3n)^{207}Bi	18.23	26.8
95	30067	103	^{67}Zn(n,p)^{67}Cu	4.7091	0.8	139	69169	17	^{169}Tm(n,3n)^{167}Tm	18.5	29.8
151	82204	82204m	^{204}Hg(n,n')^{204m}Hg	5.0415	1	77	27059	17	^{59}Co(n,3n)^{57}Co	22.38	75.7
110	42092	41092m	^{92}Mo(n,X)^{92m}Nb	5.3911	1	154	83209	37	^{209}Bi(n,4n)^{206}Bi	26.6	75.7
109	42000	41092m	^{nat}Mo(n,X)^{92m}Nb	5.3912	1	155	83209	152	^{209}Bi(n,5n)^{205}Bi	29.75	75.7
39	13027	103	^{27}Al(n,p)^{27}Mg	5.8427	1.2						

Table III: This table is derived from Table II. The only difference is that a duplicate entry has been eliminated from each highlighted pair in Table II. Retained entries remain highlighted.

No.	Mat.	MT	Reaction	E (50%) MeV	Unc. Sp. [%]	No.	Mat.	MT	Reaction	E (50%) MeV	Unc. Sp. [%]
26	5010	801	$^{10}B(n,\alpha_1)^{7}Li$	0.42562	1.01	39	13027	103	$^{27}Al(n,p)^{27}Mg$	5.84274	1.15
51	21045	102	$^{45}Sc(n,\gamma)^{46}Sc$	0.56682	1.07	79	27059	103	$^{59}Co(n,p)^{59}Fe$	5.94299	1.16
105	41093	102	$^{93}Nb(n,\gamma)^{94}Nb$	0.65159	0.92	13	3007	207	$^{7}Li(n,t)^{4}He$	6.00577	1.23
7	3006	105	$^{6}Li(n,t)^{4}He$	0.65237	0.55	54	22046	103	$^{46}Ti(n,p)^{46}Sc$	6.08127	1.19
149	79197	102	$^{197}Au(n,\gamma)^{198}Au$	0.72409	0.74	85	28060	103	$^{60}Ni(n,p)^{60}Co$	7.05428	1.37
73	26058	102	$^{58}Fe(n,\gamma)^{59}Fe$	0.73382	0.65	44	14028	103	$^{28}Si(n,p)^{28}Al$	7.2258	1.43
114	47109	47110m	$^{109}Ag(n,\gamma)^{110m}Ag$	0.73434	0.53	91	29063	107	$^{63}Cu(n,\alpha)^{60g}Co$	7.27355	1.38
63	25055	102	$^{55}Mn(n,\gamma)^{56}Mn$	0.74967	1.33	69	26054	107	$^{54}Fe(n,\alpha)^{51}Cr$	7.42963	1.42
142	73181	102	$^{181}Ta(n,\gamma)^{182}Ta$	0.81826	0.77	70	26056	103	$^{56}Fe(n,p)^{56}Mn$	7.57906	1.46
22	5010	107	$^{10}B(n,\alpha)^{7}Li$	0.89788	0.57	164	92238	16	$^{238}U(n,2n)^{237}U$	8.20773	1.6
159	90232	102	$^{232}Th(n,\gamma)^{233}Th$	0.90132	0.45	37	12024	103	$^{24}Mg(n,p)^{24}Na$	8.26047	1.59
78	27059	102	$^{59}Co(n,\gamma)^{60}Co$	0.90285	0.9	36	12000	11024g	$^{nat}Mg(n,X)^{24g}Na$	8.26095	1.59
166	92238	102	$^{238}U(n,\gamma)^{239}U$	0.91877	0.48	56	22048	103	$^{48}Ti(n,p)^{48}Sc$	8.35358	1.57
90	29063	102	$^{63}Cu(n,\gamma)^{64}Cu$	0.96389	0.62	80	27059	107	$^{59}Co(n,\alpha)^{56}Mn$	8.37156	1.56
35	11023	102	$^{23}Na(n,\gamma)^{24}Na$	1.00585	0.83	40	13027	107	$^{27}Al(n,\alpha)^{24}Na$	8.66807	1.63
145	74186	102	$^{186}W(n,\gamma)^{187}W$	1.02268	0.45	152	83209	16	$^{209}Bi(n,2n)^{208}Bi$	9.86634	1.87
129	49115	49116g	$^{115}In(n,\gamma)^{116g}In$	1.04333	0.42	57	23051	107	$^{51}V(n,\alpha)^{48}Sc$	9.97529	1.89
123	49113	49114g	$^{113}In(n,\gamma)^{114g}In$	1.09394	0.46	138	69169	16	$^{169}Tm(n,2n)^{168}Tm$	10.382	1.99
133	57139	102	$^{139}La(n,\gamma)^{140}La$	1.29321	0.48	148	79197	16	$^{197}Au(n,2n)^{196}Au$	10.5422	2.02
118	49000	49114m	$^{nat}In(n,\gamma)^{114m}In$	1.36123	0.46	107	41093	41092m	$^{93}Nb(n,2n)^{92m}Nb$	11.3282	2.23
24	5010	207	$^{10}B(n,X)^{4}He$	1.47677	0.44	30	5011	207	$^{11}B(n,X)^{4}He$	11.4595	2.27
18	5000	207	$^{nat}B(n,X)^{4}He$	1.4856	0.44	130	53127	16	$^{127}I(n,2n)^{126}I$	11.5795	2.33
161	92235	18	$^{235}U(n,fission)$	1.70344	0.06	128	49115	49114m	$^{115}In(n,2n)^{114m}In$	11.8082	2.42
9	3006	207	$^{6}Li(n,X)^{4}He$	1.70993	0.4	134	59141	16	$^{141}Pr(n,2n)^{140}Pr$	11.8459	2.45
172	94239	18	$^{239}Pu(n,fission)$	1.77434	0.04	92	29065	16	$^{65}Cu(n,2n)^{64}Cu$	12.6796	2.97
25	5010	800	$^{10}B(n,\alpha_0)^{7}Li$	1.81743	0.2	29	5011	205	$^{11}B(n,X)^{3}H$	12.8385	3.22
169	93237	18	$^{237}Np(n,fission)$	2.0527	0.21	99	33075	16	$^{75}As(n,2n)^{74}As$	12.9142	3.17
175	95241	18	$^{241}Am(n,fission)$	2.22681	0.29	62	25055	16	$^{55}Mn(n,2n)^{54}Mn$	12.9165	3.16
111	45103	45103m	$^{103}Rh(n,n')^{103m}Rh$	2.37843	0.25	76	27059	16	$^{59}Co(n,2n)^{58}Co$	13.0897	3.33
127	49115	49115m	$^{115}In(n,n')^{115m}In$	2.67343	0.37	89	29063	16	$^{63}Cu(n,2n)^{62}Cu$	13.8404	4.29
106	41093	41093m	$^{93}Nb(n,n')^{93m}Nb$	2.68481	0.35	100	39089	16	$^{89}Y(n,2n)^{88}Y$	13.9015	4.35
122	49113	49113m	$^{113}In(n,n')^{113m}In$	2.73029	0.39	31	9019	16	$^{19}F(n,2n)^{18}F$	14.0522	4.67
165	92238	18	$^{238}U(n,fission)$	2.76849	0.39	102	40090	16	$^{90}Zr(n,2n)^{89}Zr$	14.4235	5.31
158	90232	18	$^{232}Th(n,fission)$	3.00637	0.42	59	24000	24051g	$^{nat}Cr(n,X)^{51g}Cr$	14.7195	5.9
150	80199	80199m	$^{199}Hg(n,n')^{199m}Hg$	3.09845	0.43	83	28058	16	$^{58}Ni(n,2n)^{57}Ni$	14.9857	6.67
46	15031	103	$^{31}P(n,p)^{31}Si$	3.73196	0.65	98	30068	29067g	$^{68}Zn(n,X)^{67g}Cu$	15.5657	9.91
23	5010	205	$^{10}B(n,X)^{3}H$	3.73456	0.51	34	11023	16	$^{23}Na(n,2n)^{22}Na$	15.5953	8.43
55	22047	103	$^{47}Ti(n,p)^{47}Sc$	3.81716	0.61	42	13027	13026g	$^{27}Al(n,2n)^{26g}Al$	15.9694	9.4
3	3000	205	$^{nat}Li(n,X)^{3}H$	4.00588	0.66	45	14029	13028g	$^{29}Si(n,X)^{28g}Al$	16.106	10.85
48	16032	103	$^{32}S(n,p)^{32}P$	4.07412	0.72	53	22046	16	$^{46}Ti(n,2n)^{45}Ti$	16.1202	10.08
4	3000	207	$^{nat}Li(n,X)^{4}He$	4.08303	0.65	38	13027	16	$^{27}Al(n,2n)^{26}Al$	16.1556	10.62
94	30064	103	$^{64}Zn(n,p)^{64}Cu$	4.16697	0.78	67	26054	16	$^{54}Fe(n,2n)^{53}Fe$	16.6092	11.87
84	28058	103	$^{58}Ni(n,p)^{58}Co$	4.20306	0.74	153	83209	17	$^{209}Bi(n,3n)^{207}Bi$	18.2255	26.79
68	26054	103	$^{54}Fe(n,p)^{54}Mn$	4.43835	0.81	139	69169	17	$^{169}Tm(n,3n)^{167}Tm$	18.4969	29.77
95	30067	103	$^{67}Zn(n,p)^{67}Cu$	4.70905	0.81	77	27059	17	$^{59}Co(n,3n)^{57}Co$	22.3768	75.74
151	82204	82204m	$^{204}Hg(n,n')^{204m}Hg$	5.04147	0.98	154	83209	37	$^{209}Bi(n,4n)^{206}Bi$	26.6004	75.74
110	42092	41092m	$^{92}Mo(n,X)^{92m}Nb$	5.39114	1.02	155	83209	152	$^{209}Bi(n,5n)^{205}Bi$	29.75	75.74

Figure 1 (**Plot 1**) is a plot of all the data included in Table III. It appears from this graphical representation that the data in Table III for energies $E_{50\%}$ > 20 MeV seem to be unreasonable, so they are ignored in the ensuing discussion. This is not surprising since both the reaction cross sections and the ^{252}Cf s.f. neutron spectrum are poorly known at these high energies, and their corresponding uncertainties are very large. Otherwise, the variation of Unc. Sp. vs. $E_{50\%}$ appears to be relatively smooth, at least at the vertical scale level of this plot, and it exhibits an increasing tendency of uncertainty with $E_{50\%}$, which is intuitively expected.

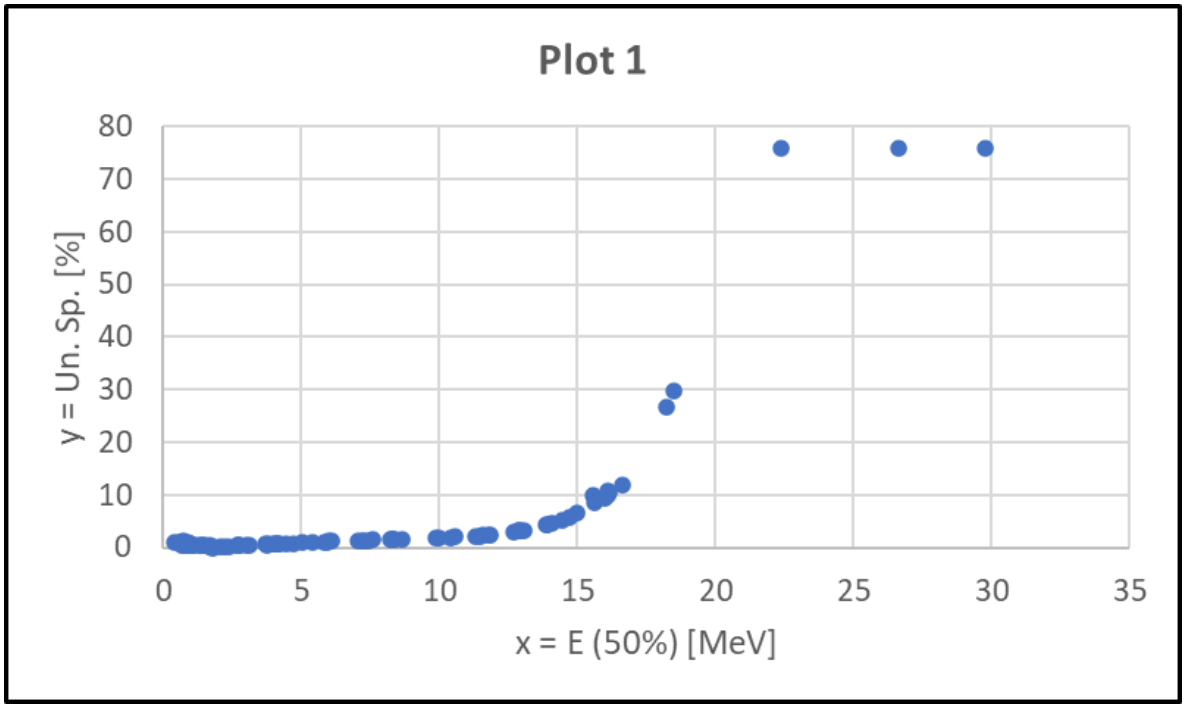

FIG. 1. *A plot (**Plot 1**) of the entire data set from Table III.*

Figure 2 (**Plot 2**) provides a closer look at the behavior of Unc. Sp. vs. $E_{50\%}$. In this figure, all data points from Table III are included except for those involving values of $E_{50\%}$ greater than 20 MeV. The plotted values are fitted by a trendline generated using an algorithm contained in Excel. A detailed discussion of the mathematical formalism used by Excel is not readily available, but it is claimed to be a form of statistical-regression analysis. The 4th-order (quartic) polynomial shown, along with the fitting formula, yields a visually decent guide to the plotted data points. The value shown in the figure for parameter R^2 generated by Excel is close to unity. According to Excel this signifies that the fitted polynomial offers a very good representation of the plotted data points. In turn, this suggests that the formula which appears in Fig. 2 could be used with considerable reliability to calculate values of Unc. Sp. for a considerable range of $E_{50\%}$ values, possibly even for reactions not included in Table III.

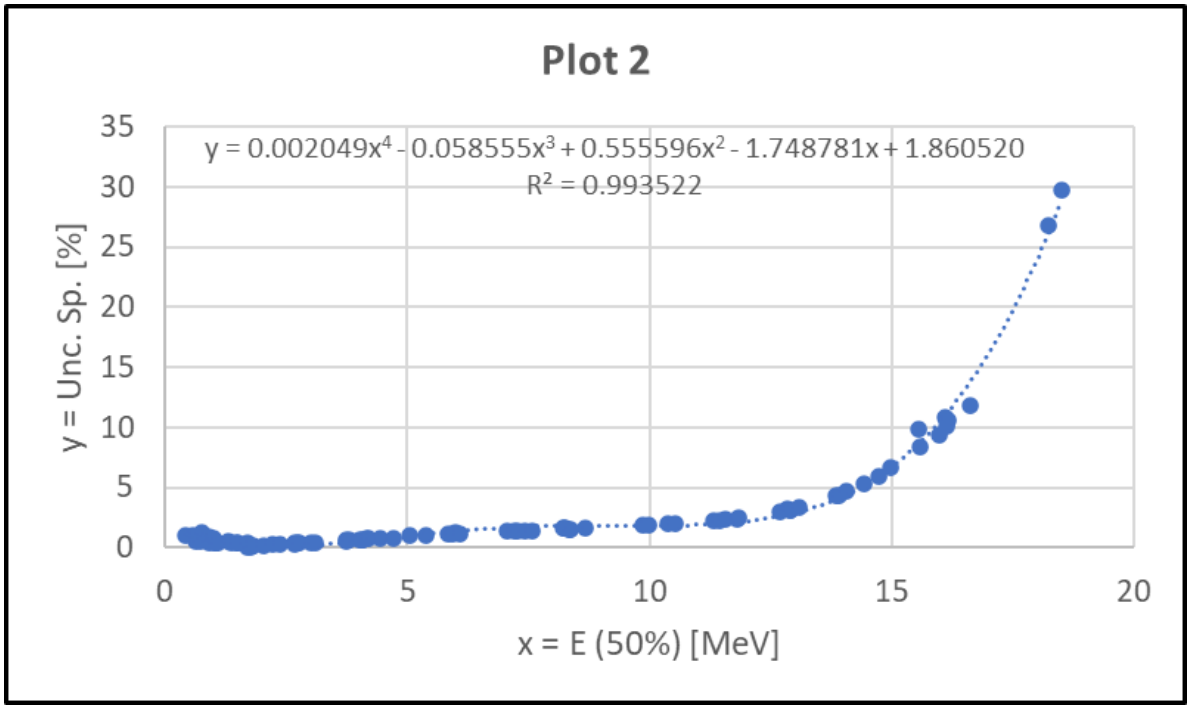

FIG. 2. *A plot (**Plot 2**) of all data from Table III minus data points with E (50%) > 20 MeV. A polynomial trendline fit to the data and its formula are shown.*

Figure 3 is a plot (**Plot 3**) of data from Table III for energies $E_{50\%}$ below 17 MeV. Again, a decent polynomial fit to these data points is provided by Excel, with a resultant R^2 close to unity. It is evident that the values of Unc. Sp. vs. $E_{50\%}$ vary quite smoothly with little scatter for energies $E_{50\%}$ above around 2 MeV, with one exception. Data point Nos. 34 and 98 both possess values of $E_{50\%}$ that are very close to each other in the vicinity of 15.6 MeV. However, their values of Unc. Sp. differ noticeably. In particular, the value of Unc. Sp. for data point No. 98, corresponding to ^{68}Zn(n,X)^{67g}Cu, falls noticeably above the trendline. These two reactions differ considerably with respect to both the target element masses and reaction types involved. The reaction ^{68}Zn(n,X)^{67g}Cu can also be expressed as ^{68}Zn(n,np+d)^{67g}Cu. Thus, there are two distinct reaction processes involved for ^{68}Zn. Graphs of evaluated values for these two component reactions taken from ENDF/B/VIII.0 [4,10] appear in Fig. 4. There are no comparable experimental data available. The shapes of these two components are obviously quite different. Graphs of evaluated and experimental data for the ^{23}Na(n,2n)^{22}Na reaction are shown in Fig. 5. Since there are strong discrepancies in the experimental data, knowledge of the (n,2n) cross section for this element should be treated as uncertain. Nevertheless, data point No. 34 for the ^{23}Na(n,2n) reaction does fall close to the trendline. Given the underlying physics differences for these two data points, it is not surprising that noticeable differences in calculated Unc. Sp. values are seen for data point Nos. 34 and 98 in spite of their close values for $E_{50\%}$.

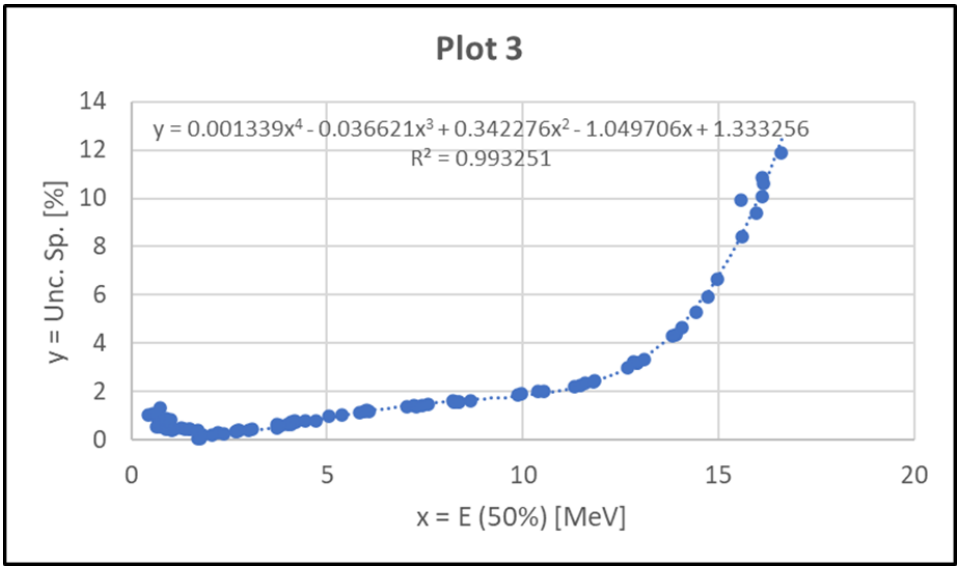

FIG. 3. *A plot (**Plot 3**) of all data from Table III minus data points with E (50%) > 17 MeV. A polynomial trendline fit to the data and its formula are shown.*

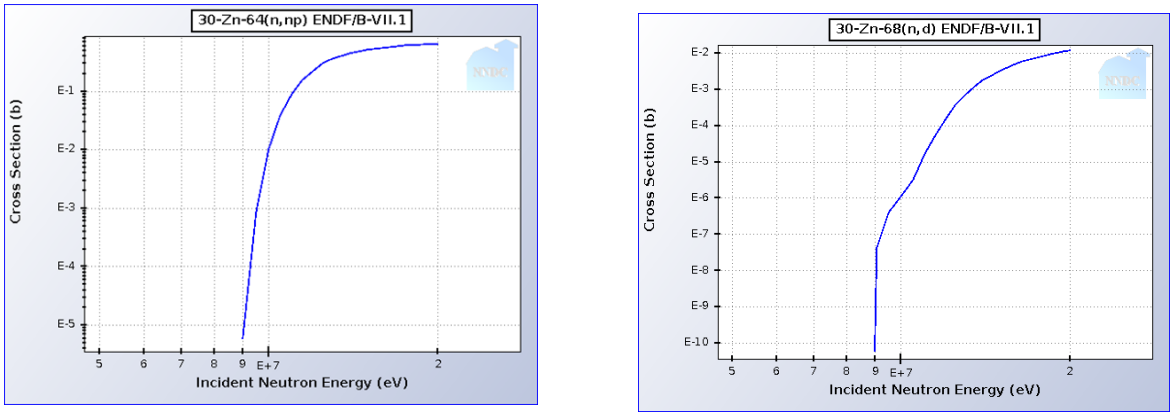

FIG. 4. *Graphs of ^{68}Zn(n,np+d)^{67g}Cu reaction cross section components [4,10]. No experimental data are available to compare with the evaluated values.*

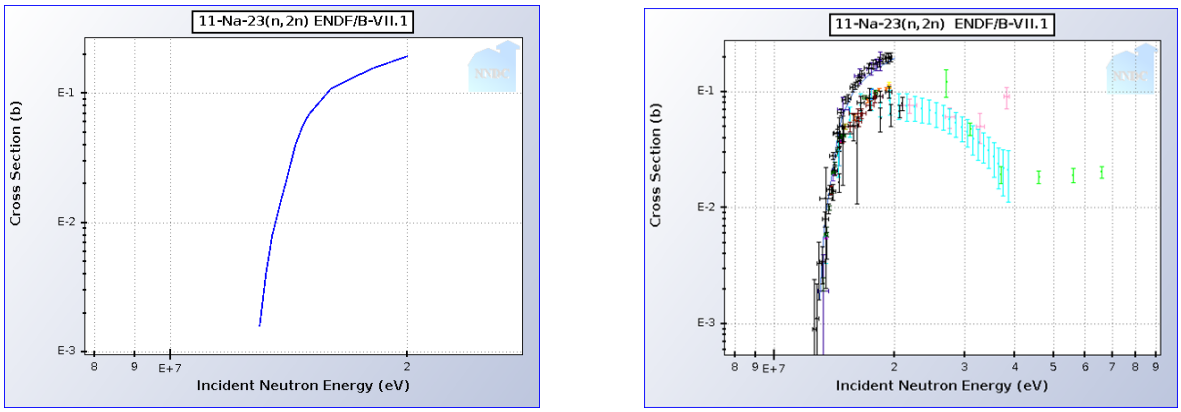

FIG. 5. *Graphs of evaluated and experimental ^{23}Na(n,2n)^{22}Na reaction cross sections [4,10]. Two graphs are provided here since the evaluated curve is difficult to see in the right-hand-side image that includes the available experimental data.*

It is instructive to graph the data from Table III separately in two distinct energy ranges: for $E_{50\%}$ values between about 2 MeV and 15 MeV and for $E_{50\%}$ values below about 2 MeV, respectively. The results appear in Figs. 6 (**Plot 4**) and 7 (**Plot 5**), respectively.

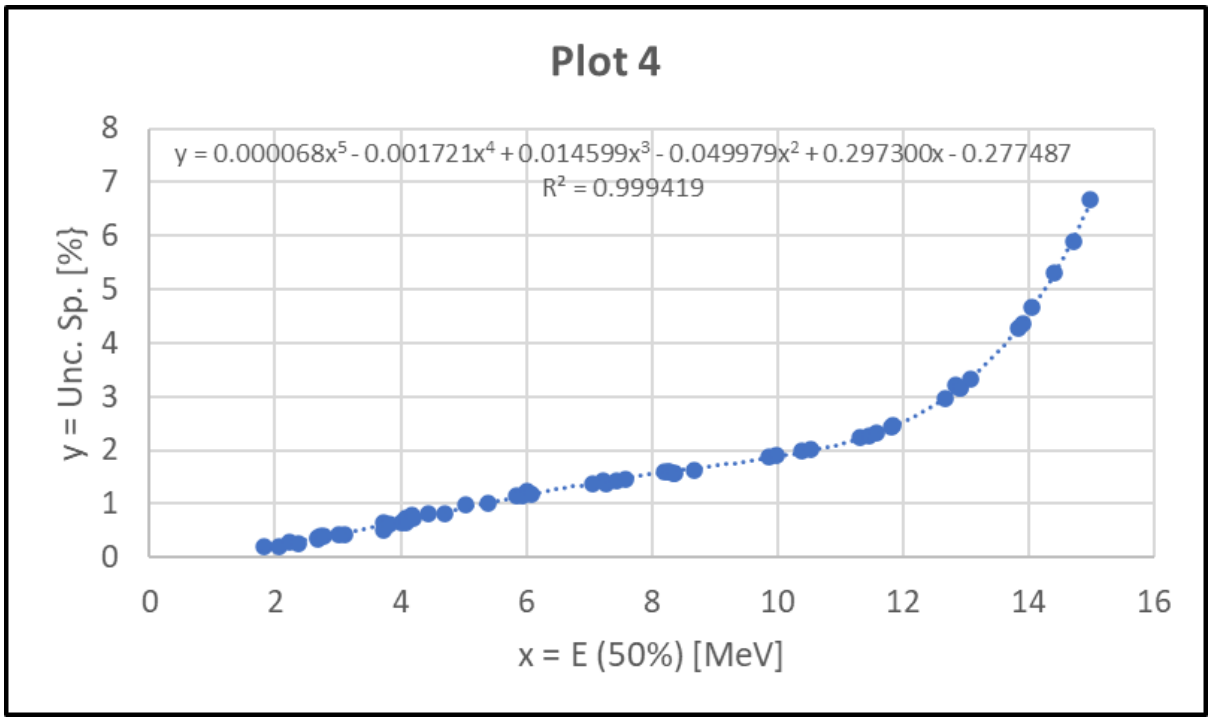

FIG. 6. *A plot (**Plot 4**) of all data from Table III for E (50%) between about 2 MeV and 15 MeV. A polynomial trendline fit to the data and its formula are shown.*

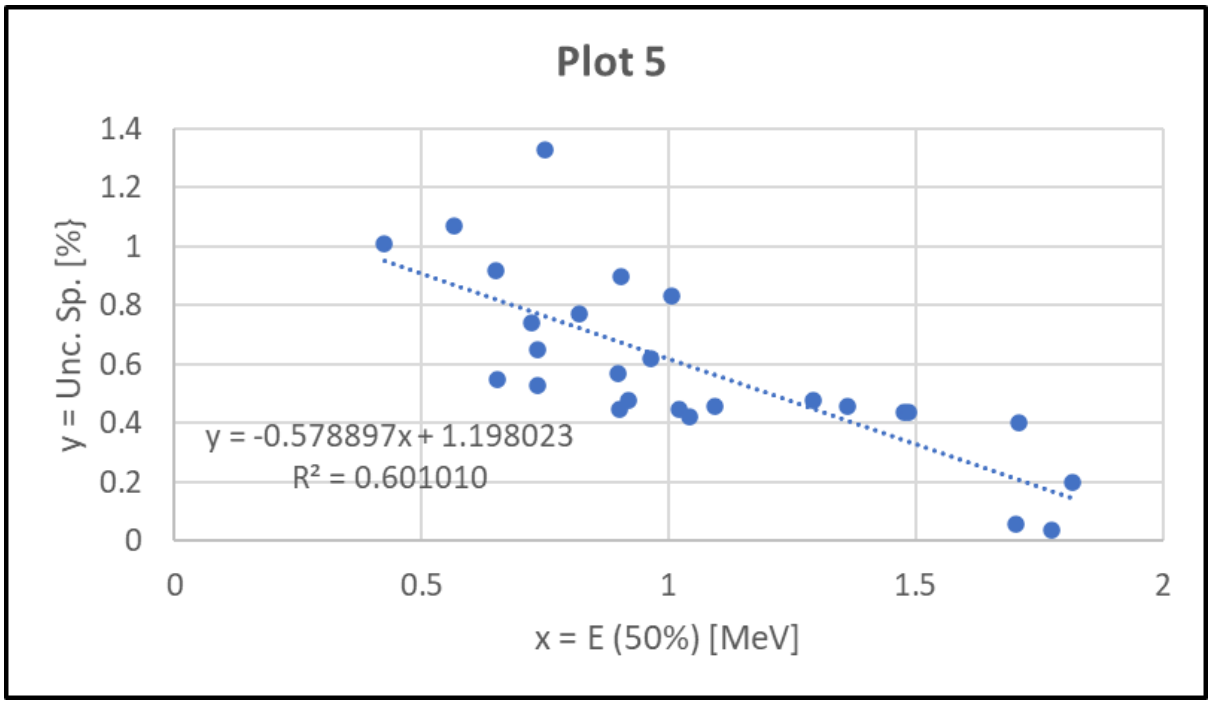

FIG. 7. *A plot (**Plot 5**) of all data from Table III for E (50%) below about 2 MeV. A polynomial trendline fit to the data and its formula are shown.*

Figure 6 (**Plot 4**) shows that the Unc. Sp. values for the data from Table III increase steadily and vary quite smoothly with increasing $E_{50\%}$ between about 2 MeV and 15 MeV. These data are represented by the indicated 5^{th}-order (quintic) polynomial trendline generated by Excel with a high degree of reliability (R^2 very close to 1). This outcome suggests that this polynomial formula might be used to estimate values of Unc. Sp. vs. $E_{50\%}$ for other reactions, regardless of their type, that have $E_{50\%}$ values falling within this range, even if they are not included in IRDFF-II. Calculated values of Unc. Sp. would appear to be relatively insensitive to details in the cross-section-excitation function shapes, and consequently they are mainly governed by the normalized ^{252}Cf s.f. neutron-spectrum-shape uncertainties over a rather wide range of $E_{50\%}$ values [1,2].

It is seen from Fig. 7 (**Plot 5**) that calculated values of Unc. Sp. vs. $E_{50\%}$ for data from Table III scatter significantly as a function of $E_{50\%}$ for reactions with $E_{50\%}$ below about 2 MeV. The linear trendline for these data generated by Excel indicates decreasing Unc. Sp. values with increasing $E_{50\%}$. An R^2 value of 0.6 signifies only a fair fit to the data. Unc. Sp. values in this region are generally smaller than 1%, and they approach close to zero for $E_{50\%}$ around 2 MeV. For these small values of Unc. Sp., the observed scatter of their values relative to the trendline is less than ± 0.5%. This trending toward very small values of Unc. Sp. around $E_{50\%}$ in the vicinity of 2 MeV is also evident from Fig. 6 (**Plot 4**) in the region of larger values of $E_{50\%}$. This is not a surprising situation since the minimum uncertainty in the evaluated ^{252}Cf s.f. neutron spectrum also occurs at around 2 MeV neutron emission energy [2,5], and this also is the region of the spectrum with the highest neutron yield.

Entries from the IRDFF-II data set that are included in Table III are comprised of several distinct reaction types. It is instructive to examine the behavior of Unc. Sp. vs. $E_{50\%}$ from Table III separately for each of these various distinct reaction types in those instances where sufficient numbers of data points are available in the specific reaction categories to justify such an undertaking. The following sections of this report address this issue.

2.1. Radiative Capture (n,γ) Reactions

Table IV gives values of Unc. Sp. vs. $E_{50\%}$ for radiative capture (n,γ) from the IRDFF-II cross-section set. This information is also presented graphically in Fig. 8 (**Plot 6**). The uncertainties range from nearly zero to 1.4%. Although they scatter considerably relative to a linear trendline fitted to the data by Excel, all but one of the tabulated Unc. Sp. values fall within about ± 0.2% of the indicated trendline. It is not surprising that scatter in these data should be observed since the reaction cross sections are comprised mainly of a 1/v component combined with resonance structure that can vary dramatically from one target nucleus to another. Since these are all small uncertainties, it may be adequate in most instances to be able to estimate the spectrum-related uncertainty contribution to the SACS from the fitted trendline.

Table IV: A subset of Table III corresponding to neutron radiative capture (n,γ) reactions.

No.	Mat.	MT	Reaction	E (50%) MeV	Unc. Sp. [%]
51	21045	102	$^{45}Sc(n,\gamma)^{46}Sc$	0.56682	1.07
105	41093	102	$^{93}Nb(n,\gamma)^{94}Nb$	0.65159	0.92
149	79197	102	$^{197}Au(n,\gamma)^{198}Au$	0.72409	0.74
73	26058	102	$^{58}Fe(n,\gamma)^{59}Fe$	0.73382	0.65
114	47109	47110m	$^{109}Ag(n,\gamma)^{110m}Ag$	0.73434	0.53
63	25055	102	$^{55}Mn(n,\gamma)^{56}Mn$	0.74967	1.33
142	73181	102	$^{181}Ta(n,\gamma)^{182}Ta$	0.81826	0.77
159	90232	102	$^{232}Th(n,\gamma)^{233}Th$	0.90132	0.45
78	27059	102	$^{59}Co(n,\gamma)^{60}Co$	0.90285	0.9
166	92238	102	$^{238}U(n,\gamma)^{239}U$	0.91877	0.48
90	29063	102	$^{63}Cu(n,\gamma)^{64}Cu$	0.96389	0.62
35	11023	102	$^{23}Na(n,\gamma)^{24}Na$	1.00585	0.83
145	74186	102	$^{186}W(n,\gamma)^{187}W$	1.02268	0.45
129	49115	49116g	$^{115}In(n,\gamma)^{116g}In$	1.04333	0.42
123	49113	49114g	$^{113}In(n,\gamma)^{114g}In$	1.09394	0.46
133	57139	102	$^{139}La(n,\gamma)^{140}La$	1.29321	0.48
118	49000	49114m	$^{nat}In(n,\gamma)^{114m}In$	1.36123	0.46

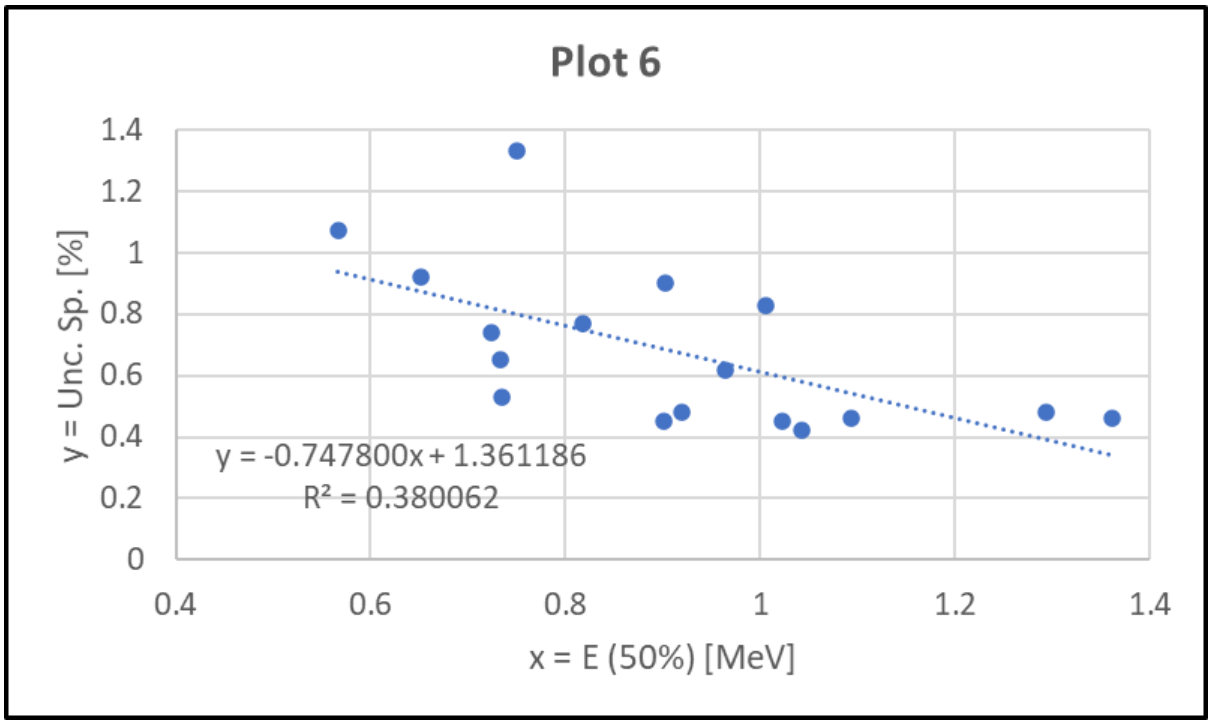

***FIG. 8**. A plot (**Plot 6**) of data for radiative capture (n,γ) reactions from Table IV. A polynomial trendline fit to the data and its formula are shown.*

2.2. (n,p) Reactions

Table V gives values of Unc. Sp. vs. $E_{50\%}$ for (n,p) reactions from the IRDFF-II cross-section set. This information is also presented graphically in Fig. 9 (**Plot 7**). The Unc. Sp. values for (n,p) reactions from the IRDFF-II cross-section set scatter modestly, and they can be fitted quite well by a 2nd-order (quadratic) polynomial. It seems likely that reliable predictions of spectrum-related uncertainties in Unc. Sp. for arbitrary (n,p) reactions with energies $E_{50\%}$ in this range could be found to within ± 0.1% using the formula shown in Fig. 9 (**Plot 7**).

Table V: A subset of Table III corresponding to (n,p) reactions.

No.	Mat.	MT	Reaction	E (50%) MeV	Unc. Sp. [%]
46	15031	103	^{31}P(n,p)^{31}Si	3.73196	0.65
55	22047	103	^{47}Ti(n,p)^{47}Sc	3.81716	0.61
48	16032	103	^{32}S(n,p)^{32}P	4.07412	0.72
94	30064	103	^{64}Zn(n,p)^{64}Cu	4.16697	0.78
84	28058	103	^{58}Ni(n,p)^{58}Co	4.20306	0.74
68	26054	103	^{54}Fe(n,p)^{54}Mn	4.43835	0.81
95	30067	103	^{67}Zn(n,p)^{67}Cu	4.70905	0.81
39	13027	103	^{27}Al(n,p)^{27}Mg	5.84274	1.15
79	27059	103	^{59}Co(n,p)^{59}Fe	5.94299	1.16
54	22046	103	^{46}Ti(n,p)^{46}Sc	6.08127	1.19
85	28060	103	^{60}Ni(n,p)^{60}Co	7.05428	1.37
44	14028	103	^{28}Si(n,p)^{28}Al	7.2258	1.43
70	26056	103	^{56}Fe(n,p)^{56}Mn	7.57906	1.46
37	12024	103	^{24}Mg(n,p)^{24}Na	8.26047	1.59
56	22048	103	^{48}Ti(n,p)^{48}Sc	8.35358	1.57

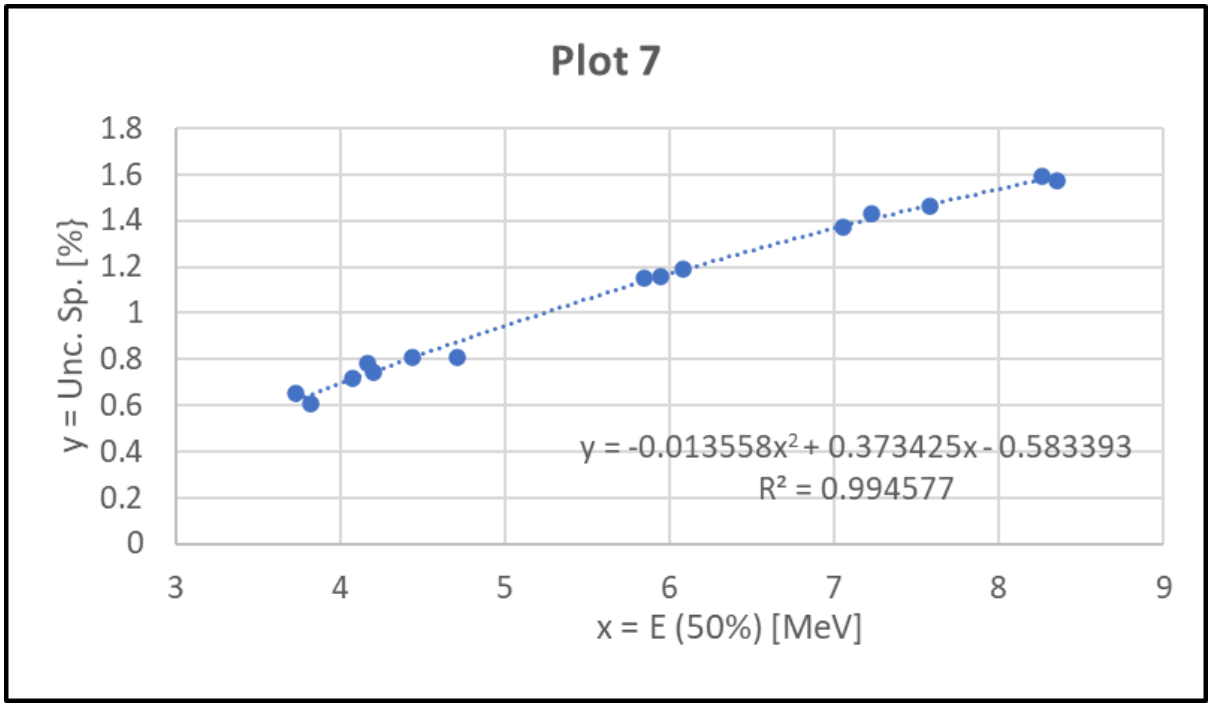

***FIG 9**. A plot (**Plot 7**) of data for (n,p) reactions from Table V. A polynomial trendline fit to the data and its formula are shown.*

2.3. (n,α) and Y(n,X)^{4}He-type Reactions

Table VI gives values of Unc. Sp. vs. $E_{50\%}$ for (n,α) and Y(n,X)^{4}He-type reactions from the IRDFF-II cross-section set. These data are plotted in Fig. 10 (**Plot 8**). Due to the distinct behavior of Unc. Sp. values vs. $E_{50\%}$ above and below around 2 MeV, it is instructive to examine these two regions by plotting their data separately in Fig. 11 (**Plot 9**) and Fig. 12 (**Plot 10**) for the low- and high- value regions of $E_{50\%}$, respectively. It is observed in Fig. 11 (**Plot 9**) that the Unc. Sp. values vs. $E_{50\%}$ scatter noticeably relative to the fitted trendline for the lower values of $E_{50\%}$, but the deviations do not exceed ±0.2%. Since these are all small uncertainties, it may be adequate to estimate the spectrum-related uncertainty contribution to the SACS for arbitrary reactions with low $E_{50\%}$ values from the fitted trendline. Fig. 12 (**Plot 10**) shows that the data for larger values of $E_{50\%}$ can be fitted quite nicely by Excel using a linear trendline, with only one value of Unc. Sp. (data point No. 13), having $E_{50\%}$ close to 6 MeV, located about 0.2% above this trendline.

Table VI: A subset of Table III corresponding to (n,α) and Y(n,X)^{4}He-type reactions.

No.	Mat.	MT	Reaction	E (50%) MeV	Unc. Sp.
26	5010	801	^{10}B(n,α$_1$)^{7}Li	0.42562	1.01
7	3006	105	^{6}Li(n,t)^{4}He	0.65237	0.55
22	5010	107	^{10}B(n,α)^{7}Li	0.89788	0.57
24	5010	207	^{10}B(n,X)^{4}He	1.47677	0.44
18	5000	207	^{nat}B(n,X)^{4}He	1.4856	0.44
9	3006	207	^{6}Li(n,X)^{4}He	1.70993	0.4
25	5010	800	^{10}B(n,α$_0$)^{7}Li	1.81743	0.2
4	3000	207	^{nat}Li(n,X)^{4}He	4.08303	0.65
13	3007	207	^{7}Li(n,t)^{4}He	6.00577	1.23
91	29063	107	^{63}Cu(n,α)^{60g}Co	7.27355	1.38
69	26054	107	^{54}Fe(n,α)^{51}Cr	7.42963	1.42
80	27059	107	^{59}Co(n,α)^{56}Mn	8.37156	1.56
40	13027	107	^{27}Al(n,α)^{24}Na	8.66807	1.63
57	23051	107	^{51}V(n,α)^{48}Sc	9.97529	1.89
30	5011	207	^{11}B(n,X)^{4}He	11.4595	2.27

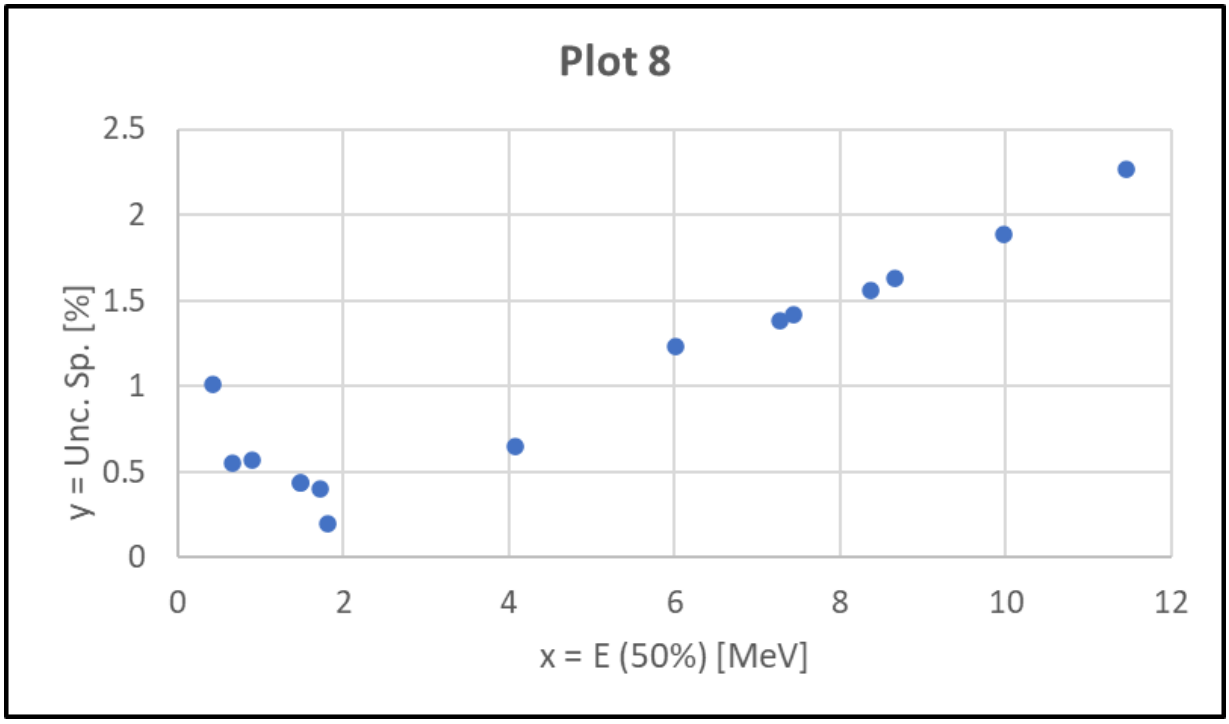

FIG. 10. *A plot (**Plot 8**) of all data for (n,α) and Y(n,X)^{4}He-type reactions from Table VI.*

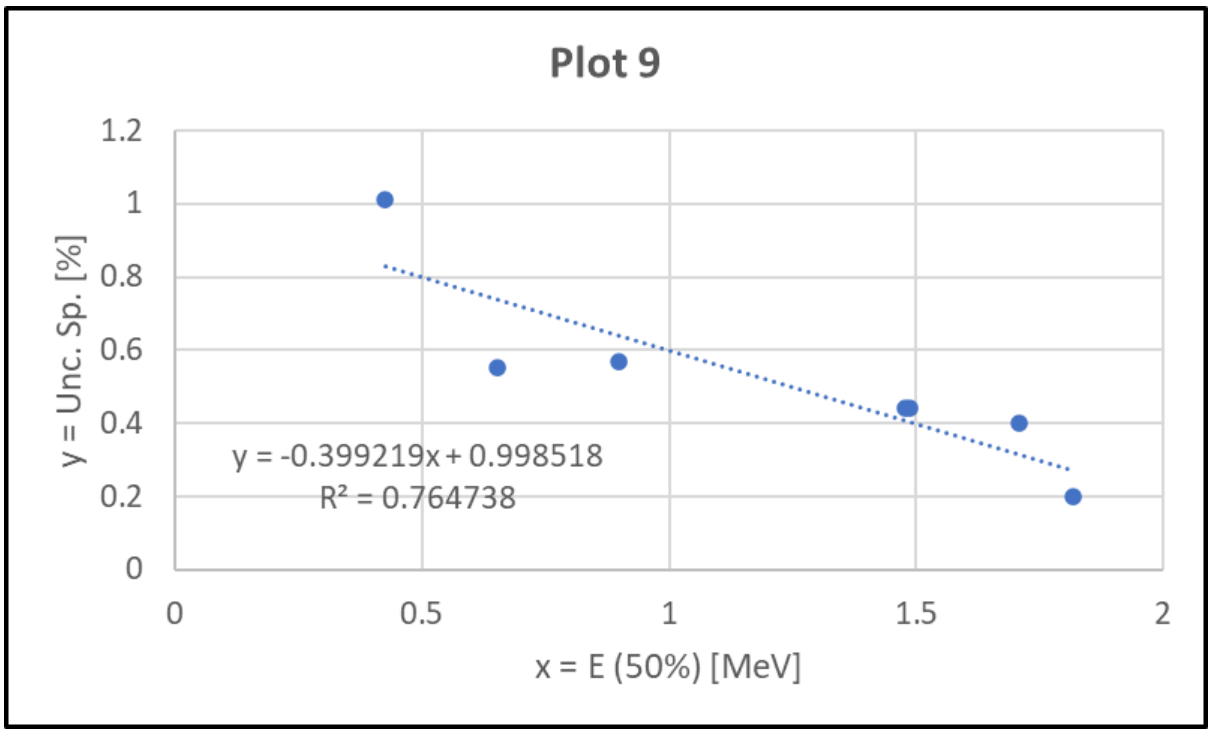

FIG. 11. *A plot (**Plot 9**) of data for (n,α) and Y(n,X)^{4}He-type reactions from Table VI for E (50%) < 2 MeV. A polynomial trendline fit to the data and its formula are shown.*

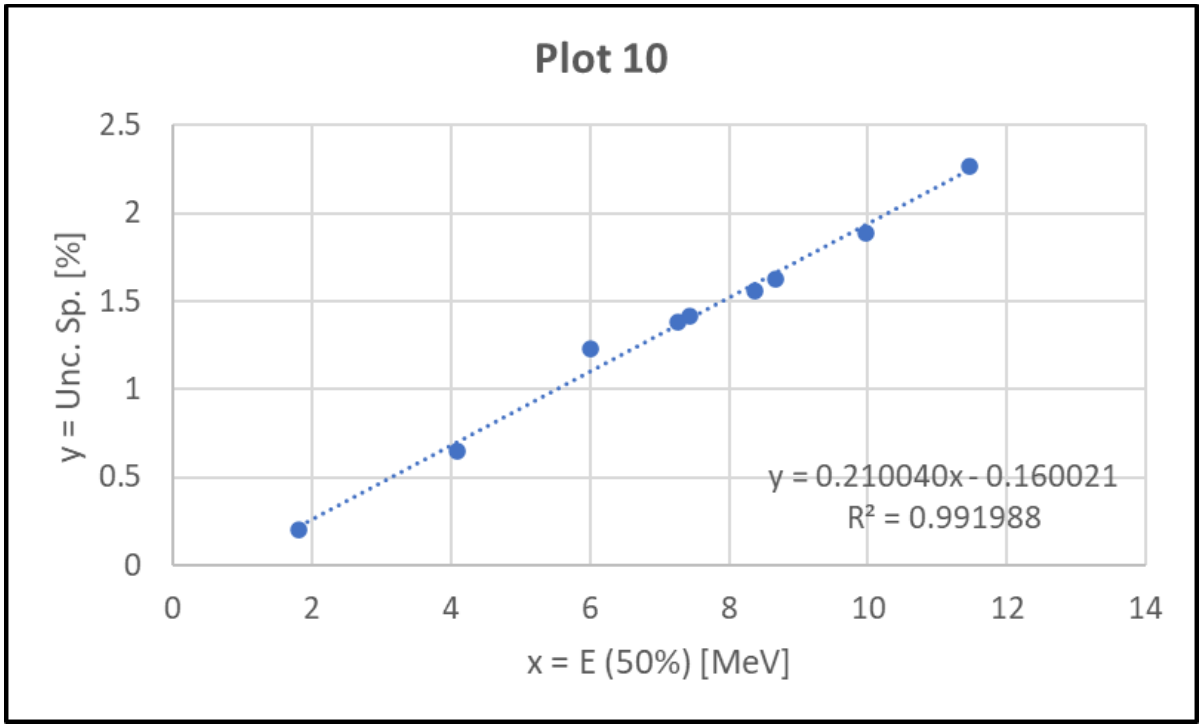

FIG. 12. *A plot (**Plot 10**) of data for (n,α) and Y(n,X)^{4}He-type reactions from Table VI for E (50%) above about 2 MeV. A polynomial trendline fit to the data and its formula are shown.*

2.4. (n,2n) Reactions

IRDFF-II includes a substantial number of (n,2n) reactions. Table VII is comprised of Unc. Sp. vs. $E_{50\%}$ data for these (n,2n) reactions, as extracted from Table III. Fig. 13 (**Plot 11**) is a plot of these data. All of these reactions have relatively high thresholds, and hence correspondingly large values of $E_{50\%}$. Also, these thresholds are well-defined, the cross sections tend to be smooth, and they increase rapidly with increasing neutron energy above their thresholds. Consequently, (n,2n) reactions are very useful for high-energy neutron dosimetry. Due to the smooth nature of (n,2n) cross sections, and their similar cross-section shapes relative to the onset of threshold, it is not surprising that Unc. Sp. vs. $E_{50\%}$ should vary smoothly with little scatter relative to the 3rd-order (cubic) polynomial trendline generated by Excel, as seen in Fig.13 (**Plot 11**).

Table VII: A subset of Table III corresponding to (n,2n) reactions.

No.	Mat.	MT	Reaction	E (50%) MeV	Unc. Sp. [%]
164	92238	16	^{238}U(n,2n)^{237}U	8.20773	1.6
152	83209	16	^{209}Bi(n,2n)^{208}Bi	9.86634	1.87
138	69169	16	^{169}Tm(n,2n)^{168}Tm	10.382	1.99
148	79197	16	^{197}Au(n,2n)^{196}Au	10.5422	2.02
107	41093	41092m	^{93}Nb(n,2n)^{92m}Nb	11.3282	2.23
130	53127	16	^{127}I(n,2n)^{126}I	11.5795	2.33
128	49115	49114m	^{115}In(n,2n)^{114m}In	11.8082	2.42
134	59141	16	^{141}Pr(n,2n)^{140}Pr	11.8459	2.45
92	29065	16	^{65}Cu(n,2n)^{64}Cu	12.6796	2.97
99	33075	16	^{75}As(n,2n)^{74}As	12.9142	3.17
62	25055	16	^{55}Mn(n,2n)^{54}Mn	12.9165	3.16
76	27059	16	^{59}Co(n,2n)^{58}Co	13.0897	3.33
89	29063	16	^{63}Cu(n,2n)^{62}Cu	13.8404	4.29
100	39089	16	^{89}Y(n,2n)^{88}Y	13.9015	4.35
31	9019	16	^{19}F(n,2n)^{18}F	14.0522	4.67
102	40090	16	^{90}Zr(n,2n)^{89}Zr	14.4235	5.31
83	28058	16	^{58}Ni(n,2n)^{57}Ni	14.9857	6.67
34	11023	16	^{23}Na(n,2n)^{22}Na	15.5953	8.43
42	13027	13026g	^{27}Al(n,2n)^{26g}Al	15.9694	9.4
53	22046	16	^{46}Ti(n,2n)^{45}Ti	16.1202	10.08
38	13027	16	^{27}Al(n,2n)^{26}Al	16.1556	10.62
67	26054	16	^{54}Fe(n,2n)^{53}Fe	16.6092	11.87

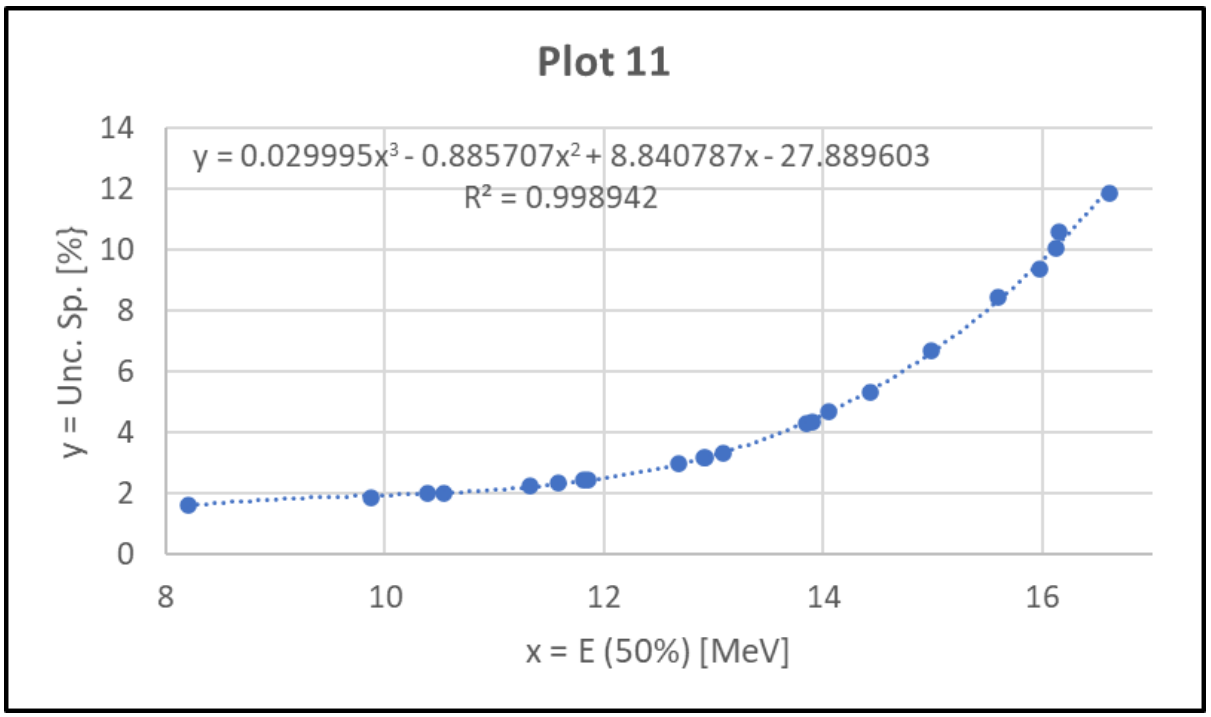

FIG. 13. *A plot (**Plot 11**) of data for (n,2n) reactions from Table VII. A polynomial trendline fit to the data and its formula are shown.*

2.5. Neutron Inelastic-Scattering (n,n') Reactions

Table VIII exhibits the data taken from the IRDFF-II set of reactions of type neutron inelastic scattering (n,n'). Fig. 14 (**Plot 12**) is a plot of these data. The number of (n,n') reactions included in the IRDFF-II set for this category of reactions is fairly limited. Since these cross sections tend to be relatively smooth, and they increase rapidly above their thresholds, one should anticipate a relatively smooth behavior of the dependence of Unc. Sp. vs. $E_{50\%}$ for these reactions stemming from the ^{252}Cf s.f. neutron-spectrum uncertainty. In fact, the 6 available data points in Fig. 14 (**Plot 12**) do suggest a systematic behavior of Unc. Sp. vs. $E_{50\%}$ for the neutron inelastic-scattering (n,n') reactions included in IRDFF-II. In fact, they are described quite well with a linear trendline generated by Excel. This linear increase of Unc. Sp. vs. $E_{50\%}$ is indicated in spite of the large gap in available data from $E_{50\%}$ just over 3 MeV up to 5 MeV. The spectrum-related uncertainties are all smaller than 1%, so reasonably reliable estimates of spectrum-related uncertainty in calculated SACS could be made for (n,n') reactions based on the Excel trendline formula shown in Fig. 14 (**Plot 12**).

Table VIII: A subset of Table III corresponding to neutron inelastic-scattering (n,n') reactions.

No.	Mat.	MT	Reaction	E (50%) MeV	Unc. Sp. [%]
111	45103	45103m	^{103}Rh(n,n')^{103m}Rh	2.37843	0.25
127	49115	49115m	^{115}In(n,n')^{115m}In	2.67343	0.37
106	41093	41093m	^{93}Nb(n,n')^{93m}Nb	2.68481	0.35
122	49113	49113m	^{113}In(n,n')^{113m}In	2.73029	0.39
150	80199	80199m	^{199}Hg(n,n')^{199m}Hg	3.09845	0.43
151	82204	82204m	^{204}Hg(n,n')^{204m}Hg	5.04147	0.98

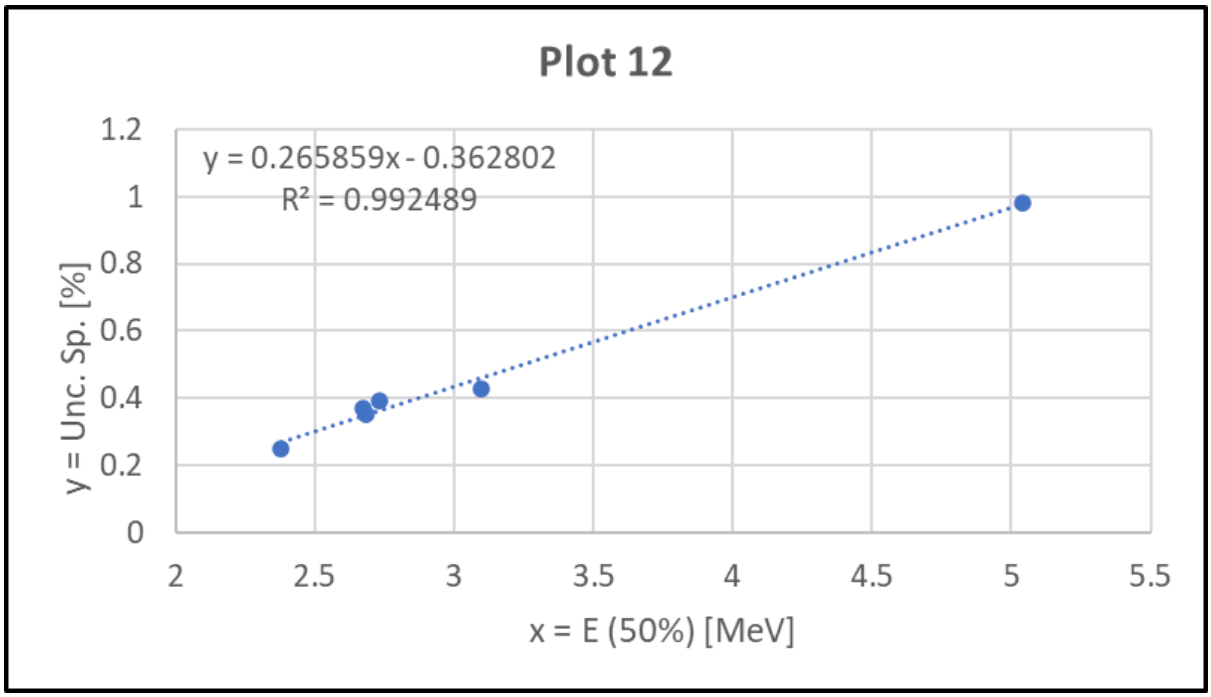

FIG. 14. *A plot (**Plot 12**) of data for neutron inelastic-scattering (n,n') reactions from Table VIII. A polynomial trendline fit to the data and its formula are shown.*

2.6. Neutron-Fission Reactions

Table IX exhibits neutron-fission SACS data taken from the IRDFF-II set of reactions. Fig. 15 (**Plot 13**) is a plot of these data. Neutron fission of actinide nuclei is a reaction process which is very important for neutron metrology in nuclear technology. Accurate measurements can be made using fission chambers as well as by radiochemical techniques [1,2]. Several distinct physical behaviors are seen in neutron fission of actinide materials, depending on the target isotopes and neutron energy ranges considered. These include 1/v, resolved-resonance, unresolved-resonance, sub-threshold fission, and smooth dependence of cross section vs. neutron energy at higher incident neutron energies. An example of evaluated and experimental cross-section data for ^{235}U is given in Fig. 16 to illustrate this point [4,10]. While it is evident from Fig. 16 that the experimental data can be very extensive, they are quite often discrepant.

For this reason, it might not be anticipated a priori that one would observe any sort of systematic behavior of Unc. Sp. vs. $E_{50\%}$ for neutron-fission reaction SACS involving the neutron spectrum of ^{252}Cf s.f. However, a plot of the five data points taken from Table IX that is presented in Fig. 15 (**Plot 13**) suggests otherwise. These data for Unc. Sp. vs. $E_{50\%}$ increase fairly consistently with increasing $E_{50\%}$, and they can be fitted by Excel reasonably well with a quadratic polynomial trendline. Departures from this trendline appear to be smaller than ± 0.02%. Furthermore, all the spectrum-related uncertainties in these fission-reaction SACS are < 0.5%. Therefore, it is reasonable to assume that the formula given in Fig. 15 (**Plot 13**) can be applied with a considerable degree of reliability to estimate the spectrum-related uncertainties for neutron-fission reaction SACS.

Table IX: A subset of Table III corresponding to neutron fission reactions.

No.	Mat.	MT	Reaction	E (50%) MeV	Unc. Sp. [%]
161	92235	18	^{235}U(n,fission)	1.70344	0.06
172	94239	18	^{239}Pu(n,fission)	1.77434	0.04
169	93237	18	^{237}Np(n,fission)	2.0527	0.21
175	95241	18	^{241}Am(n,fission)	2.22681	0.29
165	92238	18	^{238}U(n,fission)	2.76849	0.39
158	90232	18	^{232}Th(n,fission)	3.00637	0.42

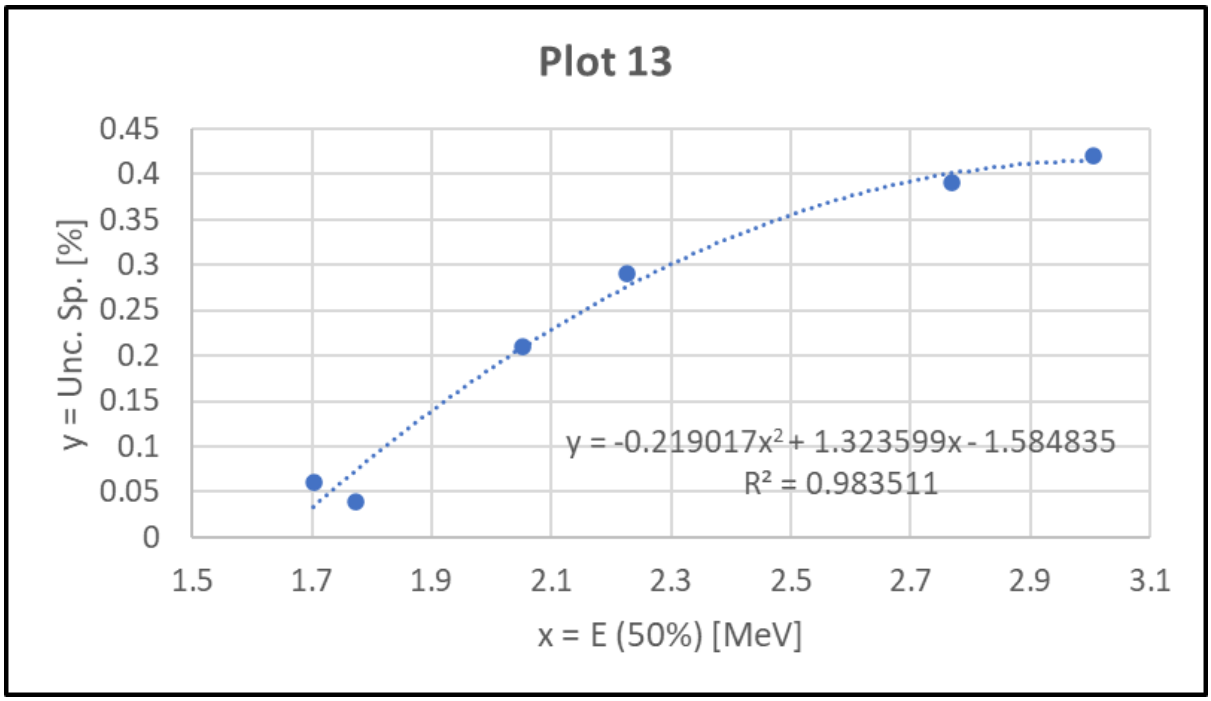

FIG. 15. *A plot (**Plot 13**) of data for neutron-fission reactions from Table IX. A polynomial trendline fit to the data and its formula are shown.*

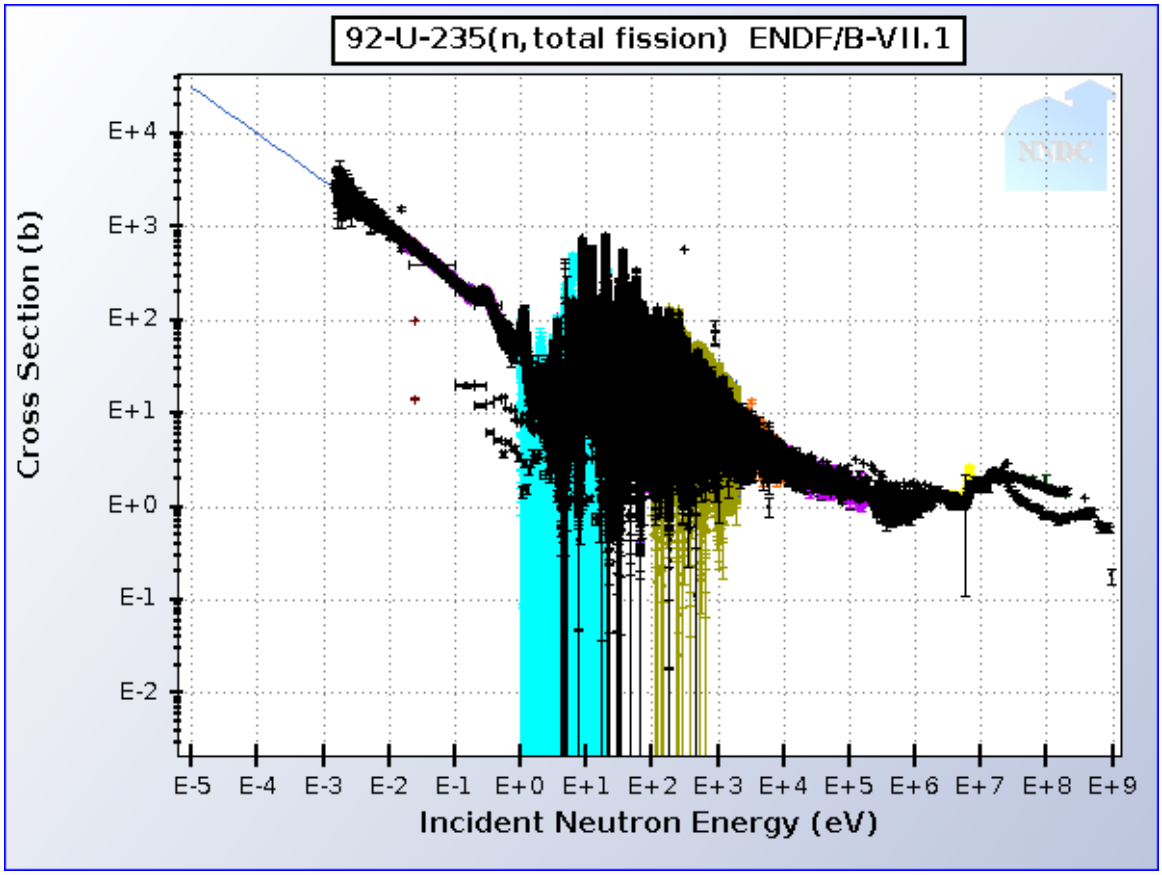

FIG. 16. *A graph of experimental and evaluated ^{235}U neutron-fission cross-sections [4,10].*

2.7. (n,t) and Y(n,X)^{3}H-type Reactions

There are 6 entries in the IRDFF-II set that correspond to (n,t) and Y(n,X)^{3}H-type reactions for the light elements Li and B. These data are present in Table X. Fig. 17 (**Plot 14**) is a plot of all these data. The data for $E_{50\%}$ above around 4 MeV suggest a linear dependence of Unc. Sp. vs. $E_{50\%}$, but the single data point (No. 7) at the lowest value of $E_{50\%}$ is clearly inconsistent with this interpretation. This data point corresponds to the reaction $^{6}Li(n,t)^{4}He$. Fig. 18 is a plot of the cross section for this reaction [4,10]. It exhibits an approximate 1/v behavior at low energies coupled with a strong, broad resonance at a neutron energy of around 240 keV. This resonance is likely the origin of the apparent anomalous behavior of data point No. 7 in Fig. 17 (**Plot 14**). The other data points in this category for IRDFF-II exhibit very different physical behaviors that are characteristic of threshold reactions. Fig. 19 (**Plot 15**) is a plot of these other data. It is evident that they can be fitted very nicely by Excel with a linear trend line. There are few elements and reactions in this light-mass-element category, each with unique physical properties, so predictability of spectrum-related uncertainties of SACS for such reactions, other than those included in IRDFF-II, may be of questionable value for practical applications.

Table X: A subset of Table III corresponding to (n,t) and Y(n,X)^{3}H-type reactions.

No.	Mat.	MT	Reaction	E (50%) MeV	Unc. Sp. [%]
7	3006	105	^{6}Li(n,t)^{4}He	0.65237	0.55
23	5010	205	^{10}B(n,X)^{3}H	3.73456	0.51
3	3000	205	^{nat}Li(n,X)^{3}H	4.00588	0.66
4	3000	207	^{nat}Li(n,X)^{4}He	4.08303	0.65
13	3007	207	^{7}Li(n,t)^{4}He	6.00577	1.23
29	5011	205	^{11}B(n,X)^{3}H	12.8385	3.22

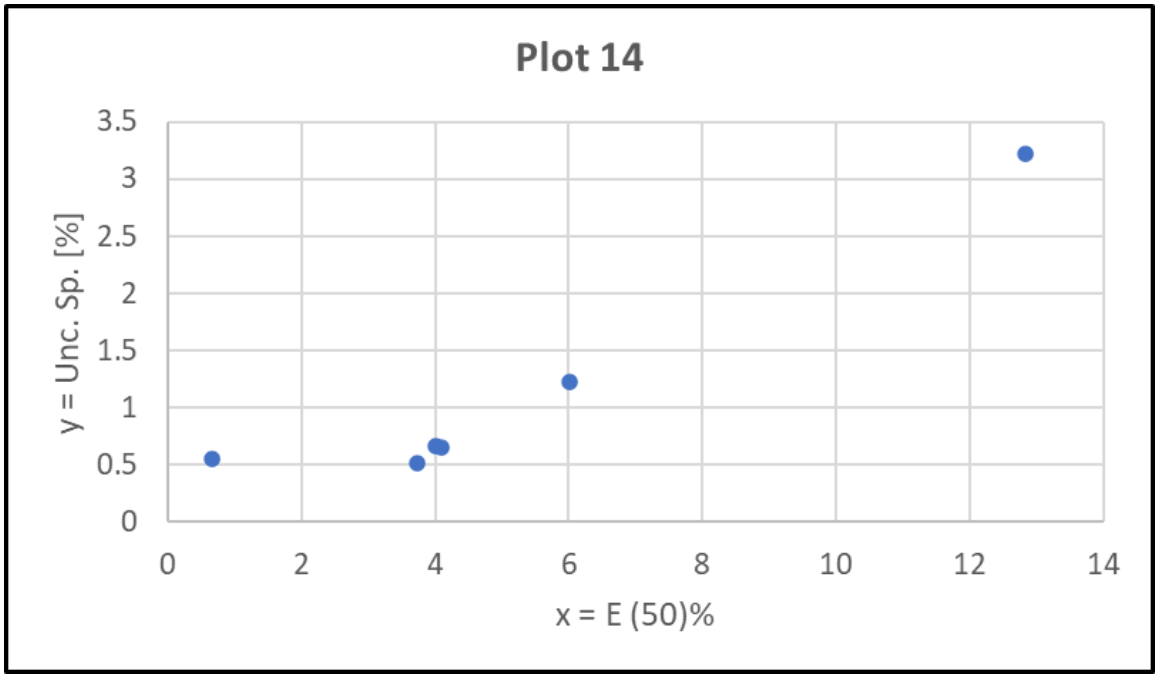

***FIG. 17**: A plot (**Plot 14**) of data for (n,t) and Y(n,X)^{3}H-type reactions from Table X.*

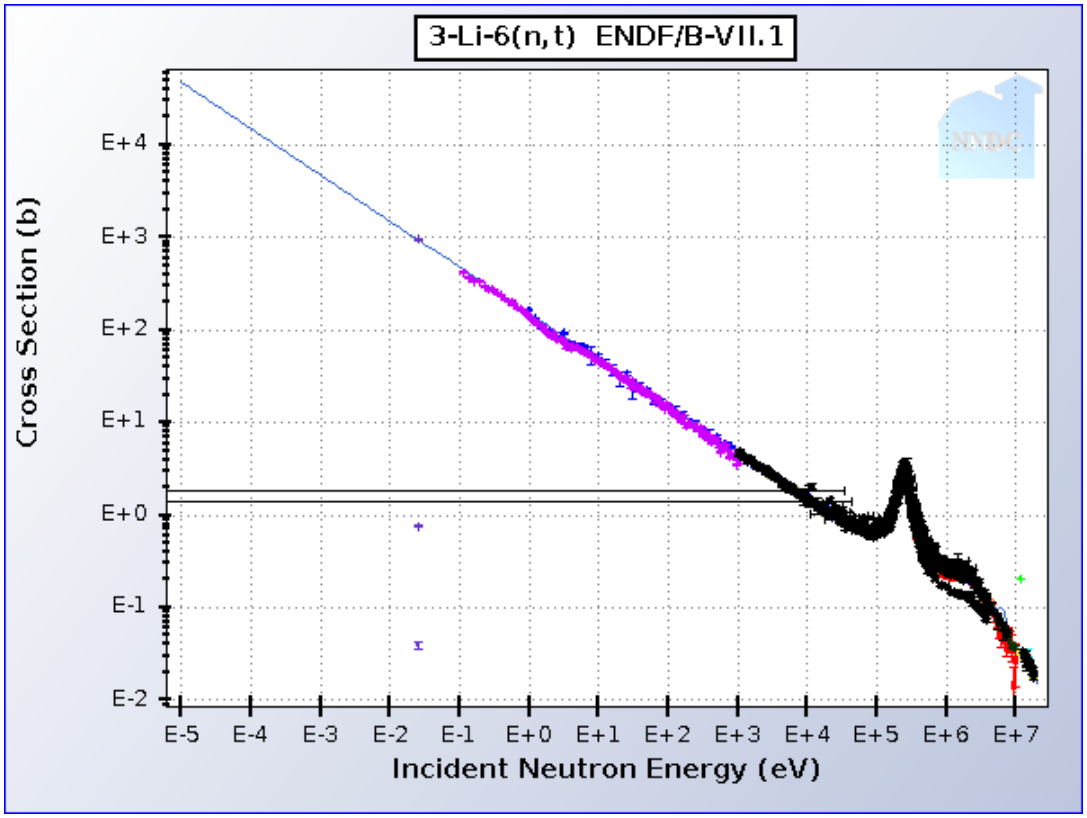

FIG. 18. *Experimental and evaluated cross-section data for the $^{6}Li(n,t)^{4}He$ reaction [4,10].*

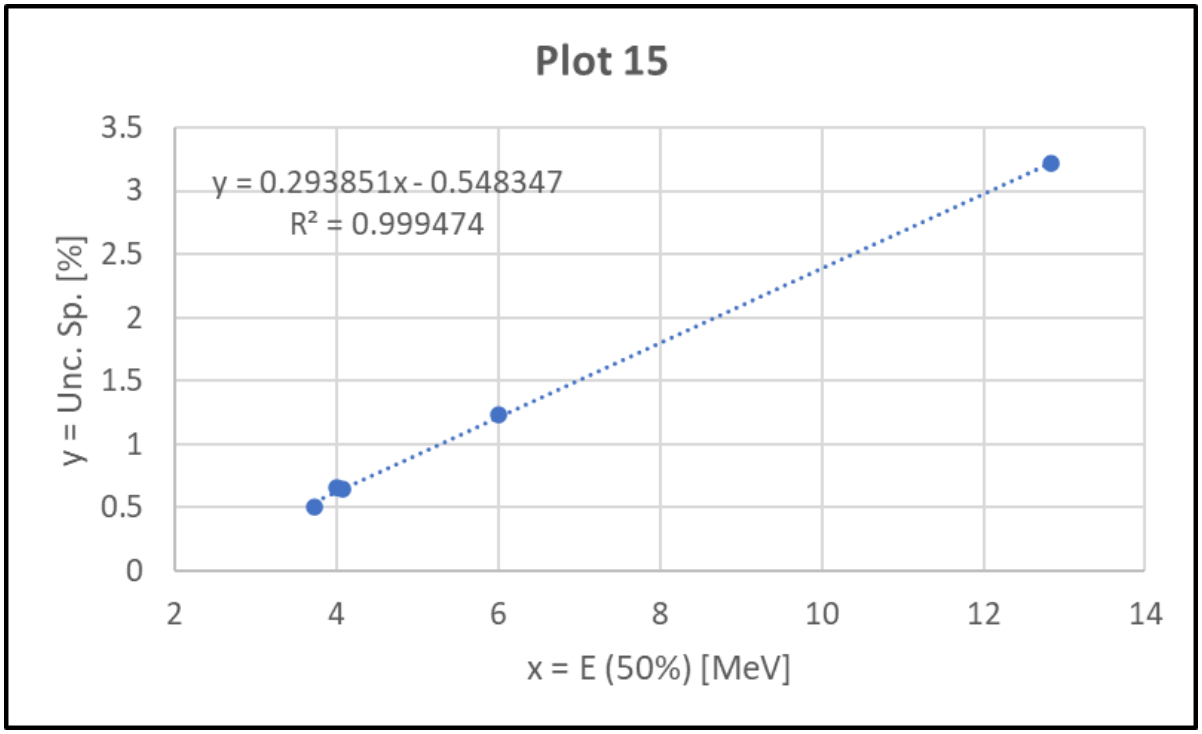

FIG. 19. *A plot (**Plot 15**) of data for (n,t) and Y(n,X)^{3}H-type reactions from Table X with data point No. 7 excluded. A polynomial trendline fit to the data and its formula are shown.*

3. Summary and Conclusions

The present work was undertaken to explore a possible existence of systematic behavior of spectrum-related SACS uncertainties as a function of the parameter $E_{50\%}$ (defined in Section 1) for measurements in the standard ^{252}Cf s.f. neutron spectrum [1,2,5]. To this end, calculated SACS data from the neutron dosimetry library IRDFF-II [1,2], generated by A. Trkov using Code RR_UNC [6], were used in the investigation. The printout from computations made using this computer code (available at the IRDFF-II website of the International Atomic Energy Agency Nuclear Data Services [2,3]) was employed, in combination with Excel, to prepare various tables and plots of spectrum-related uncertainties Unc. Sp. vs. $E_{50\%}$. Among these were tables and plots for various specific reaction types encountered in the IRDFF-II library. Smooth and predictable dependence of Unc. Sp. vs. $E_{50\%}$ is observed for all reactions when $E_{50\%}$ is greater than about 2 MeV. In this region, the data could be fitted reliable with polynomial trendlines generated by Excel. However, for SACS having $E_{50\%}$ values lower than about 2 MeV, the results are generally less predictable, for various reasons discussed in this report. At these lower $E_{50\%}$ values, the spectrum-related contributions to SACS uncertainties tend to be relatively small, so predictive capability is of much less importance. Although the observations made and conclusions drawn from the present work, are based solely on examination of data taken from the IRDFF-II database, it is suggested that they may well be more widely applicable when considering SACS data uncertainties for reactions not included in IRDFF-II.

Acknowledgment

I am indebted to Roberto Capote-Noy, IAEA Nuclear Data Section, for making me aware of the existence of code RR_XS (authored by A. Trkov) and its associated printout, as well as the availability of this information through links to the IAEA-NDS website. I also appreciate his valuable, constructive comments on the draft manuscript of the present report.

References

[1] International Reactor Dosimetry and Fusion File, IRDFF-II, Nuclear Data Services, International Atomic Energy Agency, Vienna. Website: https://www-nds.iaea.org/. (January 2020).

[2] A. Trkov et al., IRDFF-II: A New Neutron Metrology Library, Nucl. Data Sheets **163** (2020) 1-108. Also available as arXiv 1909.03336 (2019).

[3] Evaluated Nuclear Data File (ENDF-VIII.0), National Nuclear Data Center, Brookhaven National Laboratory, New York, U.S.A. Website: https://www.nndc.bnl.gov/endf/. (February 2, 2018).

[4] D.A. Brown et al., ENDF/B-VIII.0: The 8th Major Release of the Nuclear Reaction Data Library with CIELO-project Cross Sections, New Standards and Thermal Scattering Data, Nucl. Data Sheets **148** (2018) 1-148.

[5] W. Mannhart, Evaluation of the Cf-252 Fission Neutron Spectrum between 0 MeV and 20 MeV, in: Properties of Neutron Sources, Report IAEA-TECDOC-410, IAEA, Vienna, Austria (1987) 158 – 171.

[6] A. Trkov, Computer Program RR_UNC, Nuclear Data Section, International Atomic Energy Agency, Vienna, Austria. Website: https://www-nds.iaea.org/IRDFF/rr_unc.for. (Version: July 2019).

[7] R. Capote, Nuclear Data Section, International Atomic Energy Agency, Vienna, Austria, Private Communication (September 8, 2021).

[8] A. Trkov (numerical data provided by R. Capote, private communication), printout from computer program RR_UNC. Website: https://www-nds.iaea.org/IRDFF/spectra/irdff_sp_9861-Cf252_ln_RR_UNC.pdf (Version: July 2019).
[9] A. Trkov and D. Brown, ENDF-6 Formats Manual: Data Formats and Procedures for the Evaluated Nuclear Data Files. United States: N. p., 2018. Web. doi:10.2172/1425114. Website: https://www.osti.gov/biblio/1425114 (2018).
[10] Evaluated Nuclear Data File (ENDF) Retrieval & Plotting (Sigma Application), National Nuclear Data Center, Brookhaven National Laboratory, New York, U.S.A.

APPENDIX: Spectrum-Average Cross Section Uncertainties

A neutron spectrum-average cross section (SACS) S can be defined in terms of two functions $\sigma(E)$ and $\phi(E)$ of the continuous variable E by the expression

$$S = \int_{0,\infty} \sigma(E)\, \phi(E)\, dE\ , \qquad (A.1)$$

where "$\int_{0,\infty}$" signifies continuous integration between the limits $0 \le E \le \infty$, E is neutron energy, $\sigma(E)$ is the differential neutron cross section as a function of E, and $\phi(E)$ is the continuous neutron spectrum as a function of E. Furthermore, it is required that the spectrum $\phi(E)$ be normalized such that

$$\int_{0,\infty} \phi(E)\, dE = 1\ . \qquad (A.2)$$

In practice, it is common to express a SACS in terms of discrete group cross-section values σ_{gi} and normalized group fluxes ϕ_{gi} (i=1,n). A finite energy range E_{low} to E_{high} is divided into contiguous energy groups with widths ΔE_i such that

$$\sum_{i=1,n} \Delta E_i = E_{high} - E_{low}\ . \qquad (A.3)$$

A large number of contiguous groups n are defined, the individual energy-group interval widths ΔE_i are chosen to be small (consistent with typical variations of σ and ϕ with E), and energy limits E_{low} and E_{high} are selected such that the product $\sigma(E)\, \phi(E)$ is vanishingly small for all $E < E_{low}$ and $E > E_{high}$. By this means it is possible to satisfy the following approximations to any desired level of accuracy:

$$\sum_{i=1,n} \sigma_{gi}\, \phi_{gi} \approx \int_{0,\infty} \sigma(E)\, \phi(E)\, dE \qquad (A.4)$$

and

$$\sum_{i=1,n} \phi_{gi} \approx \int_{0,\infty} \phi(E)\, dE = 1. \qquad (A.5)$$

The i-th group cross section σ_{gi} is defined here as

$$\sigma_{gi} = [\, \int\{E_{li},E_{hi}\}\, \sigma(E)\, \phi(E)\, dE\,] \,/\, \int\{E_{li},E_{hi}\}\, \phi(E)\, dE\,]\ , \qquad (A.6)$$

where $\int\{E_{li},E_{hi}\}$signifies integration over the energy interval $E_{li} \le E \le E_{hi}$ with width ΔE_i , beginning at energy E_{li} and ending at energy E_{hi}. In this scheme, $\Delta E_i = E_{hi} - E_{li}$, $E_{l1} = E_{low}$, $E_{hn} = E_{high}$. So, σ_{gi} is clearly the spectrum-weighted, group-average cross-section value for the i-th energy interval of the spectrum.

The i-th normalized-spectrum group flux ϕ_{gi} is defined here as

$$\phi_{gi} = \int\{E_{li},E_{hi}\}\, \phi(E)\, dE\ . \qquad (A.7)$$

The notation here, as well as the integration ranges and energy limits, are as described above.

The uncertainty in the SACS value S is defined in terms of its variance var(S). It depends on the collection of group-average cross-section values $\boldsymbol{\sigma}_g$ and their covariance matrix $\mathbf{V}_{\sigma g}$, as well as on the collection of normalized spectrum group fluxes $\boldsymbol{\phi}_g$ and their covariance matrix $\mathbf{V}_{\phi g}$. In the formulas given in the following discussion below, terms that are particularly relevant to the present investigation are highlighted. Note that the vector and matrix quantities appear here

in bold font notation. The quantity var(S) can be derived by linear error propagation. This corresponds to the well-known matrix formula ("Sandwich Rule")

$$\mathrm{var}(S) = \boldsymbol{\phi}_g \, \mathbf{V}_{\sigma g} \, \boldsymbol{\phi}_g^{\,t} + \boldsymbol{\sigma}_g \, \mathbf{V}_{\phi g} \, \boldsymbol{\sigma}_g^{\,t} \, . \qquad \text{(A.8)}$$

The superscript "t" signifies vector / matrix transposition. Eq. (A.8) can also be written more explicitly in the following equivalent, non-matrix algebraic formula:

$$\mathrm{var}(S) = \sum_{i,j} \phi_{gi} \, v_{\sigma gij} \, \phi_{gj} + \sum_{i,j} \sigma_{gi} \, v_{\phi gij} \, \sigma_{gj} \, . \quad (i,j=1,n) \qquad \text{(A.9)}$$

Here, $v_{\sigma gij}$ is an element of matrix $\mathbf{V}_{\sigma g}$ and $v_{\phi gij}$ is an element of matrix $\mathbf{V}_{\phi g}$. The error propagation exercise that produces var(S) results in two distinct terms because the collections of variables $\boldsymbol{\sigma}_g$ and $\boldsymbol{\phi}_g$ are treated as mutually independent in the present investigation since the uncertainties for the ^{252}Cf s.f. neutron spectrum are independent of the uncertainties for all the reaction cross sections involved in the SACS reactions relevant to IRDFF-II.

Eqs. (A.8) and (A.9) for var(S) can also be expressed symbolically as a sum of two partial variance terms in the following obvious way:

$$\mathrm{var}(S) \equiv \mathrm{var}_{tot}(S) = \mathrm{var}_{\sigma}(S) + \mathrm{var}_{\phi}(S) \, . \qquad \text{(A.10)}$$

Total and partial standard deviations in S are related to the corresponding variances by the expressions:

$$\mathrm{stdev}_{tot}(S) = [\mathrm{var}_{tot}(S)]^{½}, \qquad \text{(A.11)}$$

$$\mathrm{stdev}_{\sigma}(S) = [\mathrm{var}_{\sigma}(S)]^{½}, \qquad \text{(A.12)}$$

$$\mathrm{stdev}_{\phi}(S) = [\mathrm{var}_{\phi}(S)]^{½}. \qquad \text{(A.13)}$$

Finally, the fractional standard deviation in the SACS value S due to uncertainties in the normalized spectrum ϕ is given by the formula:

$$\mathrm{fract}\{\mathrm{stdev}_{\phi}(S)\} = \mathrm{stdev}_{\phi}(S) \, / \, S \, . \qquad \text{(A.14)}$$

Eq. (A.14) can also be expressed in percent by multiplying the right-hand-side of the equation by the factor 100.

Nuclear Data Section
International Atomic Energy Agency
Vienna International Centre, P.O. Box 100
A-1400 Vienna, Austria

E-mail: nds.contact-point@iaea.org
Fax: (43-1) 26007
Telephone: (43-1) 2600 21725
Web: http://nds.iaea.org